Enhanced convergence technique for a one
dimensional nodal model

by

Mohammed Benghanem

A Thesis Submitted to the
Graduate Faculty in Partial Fulfillment of the
Requirements for the Degree of
MASTER OF SCIENCE

Major: Nuclear Engineering

Iowa State University
Ames, Iowa

1983

TABLE OF CONTENTS

LIST OF FIGURES

Page

LIST OF TABLES

I. INTRODUCTION

Nodal models have been used extensively in nuclear reactor analysis including safety and fuel management. The importance of using nodal model was stated by Askew in the summary of a recent international meeting on nodal methods [1]:

> Coarse mesh methods have been demonstrated to be a reliable and useful tool for both reactor designers and operators in predicting the assembly to assembly variations of rating for operating reactors. The most advanced models appear to be capable of doing this with an RMS error of the order of ±2%. There is scope for further refinement in the modeling of reflectors and shrouds, and in the representations of variations of burnup within an assembly, especially at the core edge or following shuffling of edge assemblies. With improvements of this kind, the models will be capable, given good nuclear data and lattice calculations, of a predictive accuracy of the same order as that of the measurements.

The objective of this research will be to improve the convergence of a two group, one dimensional nodal model in an array of PWR fuel assemblies which simulate a slab reactor.

Even though the one dimensional model isn't realistic for practical use, it will be undertaken for the following reasons:

(1) Clarity in the technique development,

(2) Insure the convergence of the problem, and

(3) Computational efficiency.

The technique can be extended to the more complicated two and three dimensions.

II. THE ONE DIMENSIONAL NEUTRON DIFFUSION
NODAL MODEL

A. Neutron Diffusion Theory

The general form of the two group diffusion equations is given by:

$$D_1 \frac{d^2\phi_1(x)}{dx^2} - (\Sigma_{a_1} + \Sigma_{1\to2} + \frac{1}{\lambda}\nu\Sigma_{f_1})\phi_1(x) + \frac{1}{\lambda}\nu\Sigma_{f_2}\phi_2(x) = 0$$

(II-1)

$$D_2 \frac{d^2\phi_2(x)}{dx^2} - \Sigma_{a_2}\phi_2(x) + \Sigma_{1\to2}\phi_1(x) = 0 \ .$$

(II-2)

Subscripts 1 and 2 will be used to denote the quantities in the fast and thermal groups, respectively.

$\phi_1(x)$, $\phi_2(x)$ = fluxes at point x in the fast and thermal groups, respectively;

D_1, D_2 = diffusion coefficients for the fast and thermal groups, respectively;

Σ_{a_1}, Σ_{a_2} = absorption cross section for the fast and thermal groups, respectively;

$\frac{1}{\lambda}\nu\Sigma_{f_1}$, $\frac{1}{\lambda}\nu\Sigma_{f_2}$ = fission cross sections multiplied by the neutron yield per fission for the fast and thermal groups, respectively; and

$\Sigma_{1\to2}$ = removal cross section for the fast group.

The above system of equations will be solved using the nodal method.

To simplify the equations, one can write this system

as follows:

$$\frac{d^2\phi_1}{dx^2} + \alpha_1\phi_1 + \alpha_2\phi_2 = 0 \qquad (II-3)$$

$$\frac{d^2\phi_2}{dx^2} + \beta_2\phi_2 + \beta_1\phi_1 = 0 \qquad (II-4)$$

where

$$\alpha_1 = \frac{-(\Sigma_{a_1} + \Sigma_{1\to 2}) + \frac{1}{\lambda}\nu\Sigma_{f_1}}{D_1}$$

$$\alpha_2 = \frac{\nu\Sigma_{f_2}}{\lambda D_1}$$

$$\beta_1 = \frac{\Sigma_{1\to 2}}{D_2}$$

$$\beta_2 = \frac{-\Sigma_{a_2}}{D_2} \quad .$$

Furthermore, a quantity which will be frequently used is introduced here. It's called the average nodal flux defined as:

$$\bar{\phi} \equiv \frac{\int\phi(x)\ dx}{\int dx} \quad . \qquad (II-5)$$

B. The Nodal Model

The basic idea of the method rests on the Weierstrass approximation theorem [2]. Since the neutron flux is continuous over each node (or assembly), one can expand it in a polynomial series. Moreover, the choice of a polynomial expansion is due to the fact that polynomials are continuous functions easy to manipulate.

The size of the nodes is taken equal to a fuel assembly width (~20 cm).

Fig. 1 shows the nodes arrangement. The integers refer to the material types listed in the Benchmark problem [3] shown in Table 1. Note that the fuel assemblies of type 3 are control assemblies. The configuration of Fig. 1 will be called "the regular configuration."

Table 1. Benchmark fuel parameters

Material	Region	D_1	D_2	$\Sigma_{1 \to 2}$	Σ_{a_1}	Σ_{a_2}	$\nu\Sigma_{f_2}$
Fuel 1	1	1.5	0.4	0.02	0.01	0.08	0.135
Fuel 2	2	1.5	0.4	0.02	0.01	0.085	0.135
Fuel 2 + Rod	3	1.5	0.4	0.02	0.01	0.13	0.135
Reflector	4	2.0	0.3	0.04	0.0	0.01	0.0

We will use a second order polynomial expansion to show the different steps of the model. Then the technique can be extended easily to the fourth order.

Hence, the fast flux becomes:

$$\phi_1(x) = a_0 + a_1 x + a_2 x^2 \qquad (II-6)$$

and the thermal flux will be:

$$\phi_2(x) = b_0 + b_1 x + b_2 x^2 \ . \qquad (II-7)$$

Each of the polynomials will be expanded about the center
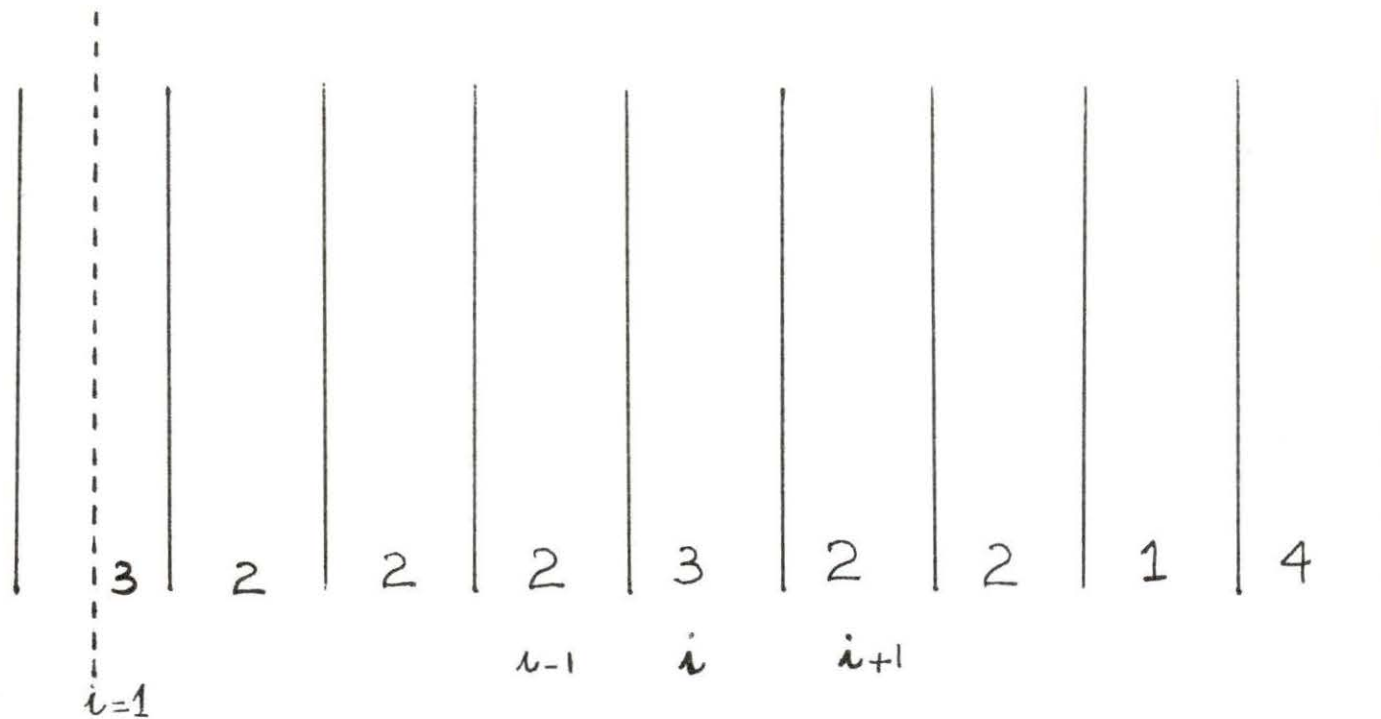
Figure 1. Half core fuel arrangement.

of the assembly (Fig. 2). Hence, equation II-5 becomes:

$$\bar{\phi}_1 = a_0 + a_2 \frac{\eta^2}{3} \qquad\qquad (II-8)$$

and

$$\bar{\phi}_2 = b_0 + b_2 \frac{\eta^2}{3} \quad . \qquad\qquad (II-9)$$

C. The Nodal Coefficient Determination

1. The second order expansion

The first concern of the model is the determination of the coefficients. They can be derived if we assume the flux values are known at the node boundaries and we apply a simple mathematical technique.

a. Determination of a_0 and a_1 In these calculations, the fast flux analysis will be developed. The thermal flux development is done in a similar manner. The flux $\phi_1(x)$ at the nodes η and $-\eta$ is assumed known and is given by:

$$\phi^\ell \equiv \phi_1(-\eta) = a_0 - a_1\eta + a_2\eta^2 \qquad\qquad (II-10)$$

and

$$\phi^r \equiv \phi_2(\eta) = a_0 + a_1\eta + a_2\eta^2 \quad . \qquad\qquad (II-11)$$

Adding these two equations, one gets:

$$a_0 = (\frac{\phi^\ell + \phi^r}{2}) - a_2\eta^2 \quad . \qquad\qquad (II-12)$$

Subtracting them, one gets:

$$a_1 = (\frac{\phi^r - \phi^\ell}{2\eta}) \quad . \qquad\qquad (II-13)$$
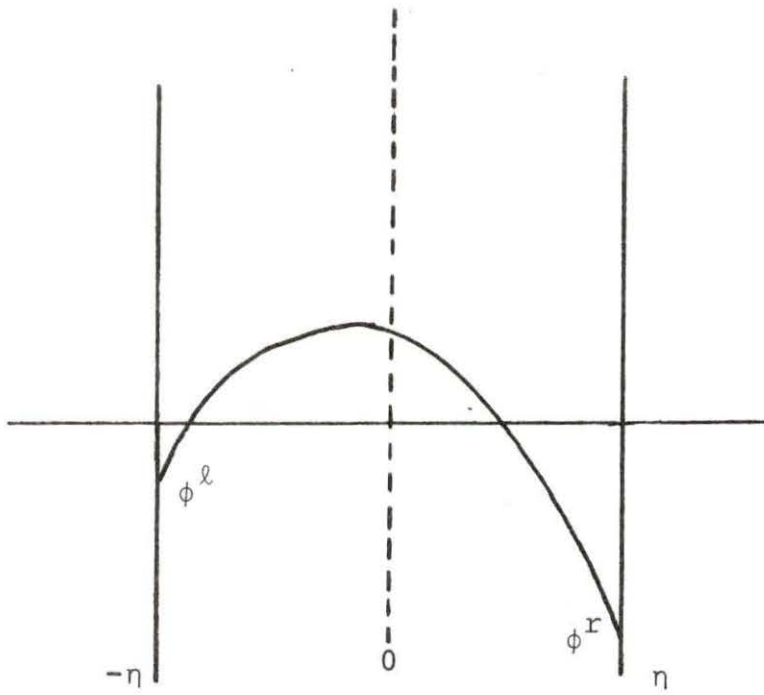
Figure 2.   Flux expansion about the center of node i

b. Use of the function g(x) to determine a_2 Substituting equation II-6 into II-3 (or equation II-7 into II-2), one can get:

$$\frac{d^2\phi_1(x)}{dx^2} = 2a_2 \quad . \tag{II-14}$$

At this stage, the function g(x) is introduced. It carries the difference between the exact and the approximate solutions.

Therefore, we will concentrate on minimizing g(x) with respect to the unknown coefficients a_2.

Substituting equation II-14 into II-3, one can get:

$$2a_2 + \alpha_1(\tilde{a}_0 + \tilde{a}_1 x + \tilde{a}_2 x^2) + \alpha_2(\tilde{b}_0 + \tilde{b}_1 x + \tilde{b}_2 x^2) = g(x) \tag{II-15}$$

where $\tilde{a}_0$, $\tilde{a}_1$, $\tilde{a}_2$ and $\tilde{b}_0$, $\tilde{b}_1$, $\tilde{b}_2$ are coefficients calculated from a previous iteration or simply:

$$2a_2 + f(x) = g(x) \tag{II-16}$$

where $f(x) = \alpha_1(\tilde{a}_0 + \tilde{a}_1 x + \tilde{a}_2 x^2) + \alpha_2(\tilde{b}_0 + \tilde{b}_1 x + \tilde{b}_2 x^2).$ $\tag{II-17}$

Therefore, minimizing g(x) in an integral sense, one can write:

$$\frac{\partial}{\partial a_2} \int_{-\eta}^{\eta} g^2(x)\,dx = 0 \tag{II-18}$$

or

$$2 \int_{-\eta}^{\eta} g(x)\,\frac{\partial g(x)}{\partial a_2}\,dx = 0 \quad . \tag{II-19}$$

Since $\frac{\partial g(x)}{\partial a_2} = 2$, equation II-18 becomes:

$$2 \int_{-\eta}^{\eta} [2a_2 + f(x)] dx = 0$$

or

$$2 \int_{-\eta}^{\eta} [2a_2 + \alpha_1 (\tilde{a}_0 + \tilde{a}_1 x + \tilde{a}_2 x^2)$$
$$+ \alpha_2 (\tilde{b}_0 + \tilde{b}_1 x + \tilde{b}_2 x^2)] dx = 0.$$

Performing the integration and arranging the terms, one gets:

$$a_2 = -\frac{1}{2}(\alpha_1 \tilde{a}_0 + \alpha_2 \tilde{b}_0) - \frac{\eta^2}{6} (\alpha_1 \tilde{a}_2 + \alpha_2 \tilde{b}_2) . \qquad \text{(II-20)}$$

c. The source calculation   Once the fluxes are found, the source term is calculated as follows:

$$S = \frac{\sum_i (\nu \Sigma_{f_1} \phi_1 + \nu \Sigma_{f_2} \phi_2) V_i}{V_T} \qquad \text{(II-21)}$$

where V_i = node individual volume and V_T = total volume of the core.

The eigenvalue or k_{eff} can be determined from:

$$k_{eff} = \frac{S^{\ell+1}}{S^{\ell}} \qquad \text{(II-22)}$$

where S^{ℓ} is the source value obtained at iteration ℓ and $S^{\ell+1}$ at the following iteration.

d. The interface calculation   To satisfy the diffusion theory requirements, the interface flux values should

be continuous:

$$\phi_i^r = \phi_{i+1}^\ell \qquad (II-23)$$

where i and i+1 represent the node indexes, ϕ^r and ϕ^ℓ are the right hand side and the left hand side flux values at the interface, as shown in Fig. 3.

To account for the continuity of the current, we introduce a function ψ at each node interface such that:

$$\frac{\phi_i^r - \psi_i^r}{\theta} = \frac{d\phi_i(x)}{dx}\Bigg|_{x=\eta} \qquad (II-24)$$

and

$$\frac{\phi_{i+1}^\ell - \psi_{i+1}^\ell}{\theta} = \frac{d\phi_{i+1}(x)}{dx}\Bigg|_{x=-\eta} \qquad (II-25)$$

where θ is any positive distance from the interface, as shown in Fig. 3.

Using equation II-6, we write for the node i:

$$\frac{d\phi_i(x)}{dx}\Bigg|_{\eta_i} = a_{1_i} + 2a_2 x_i\Bigg|_{x=\eta_i} . \qquad (II-26)$$

This can be determined from the polynomial coefficients for the node i. The relation:

$$\frac{d\phi_{i+1}(x)}{dx}\Bigg|_{\eta_{i+1}} = a_{1_{i+1}} + 2a_{2_{i+1}} x\Bigg|_{x=-\eta_{i+1}} \qquad (II-27)$$

can also be determined from the polynomial coefficients for

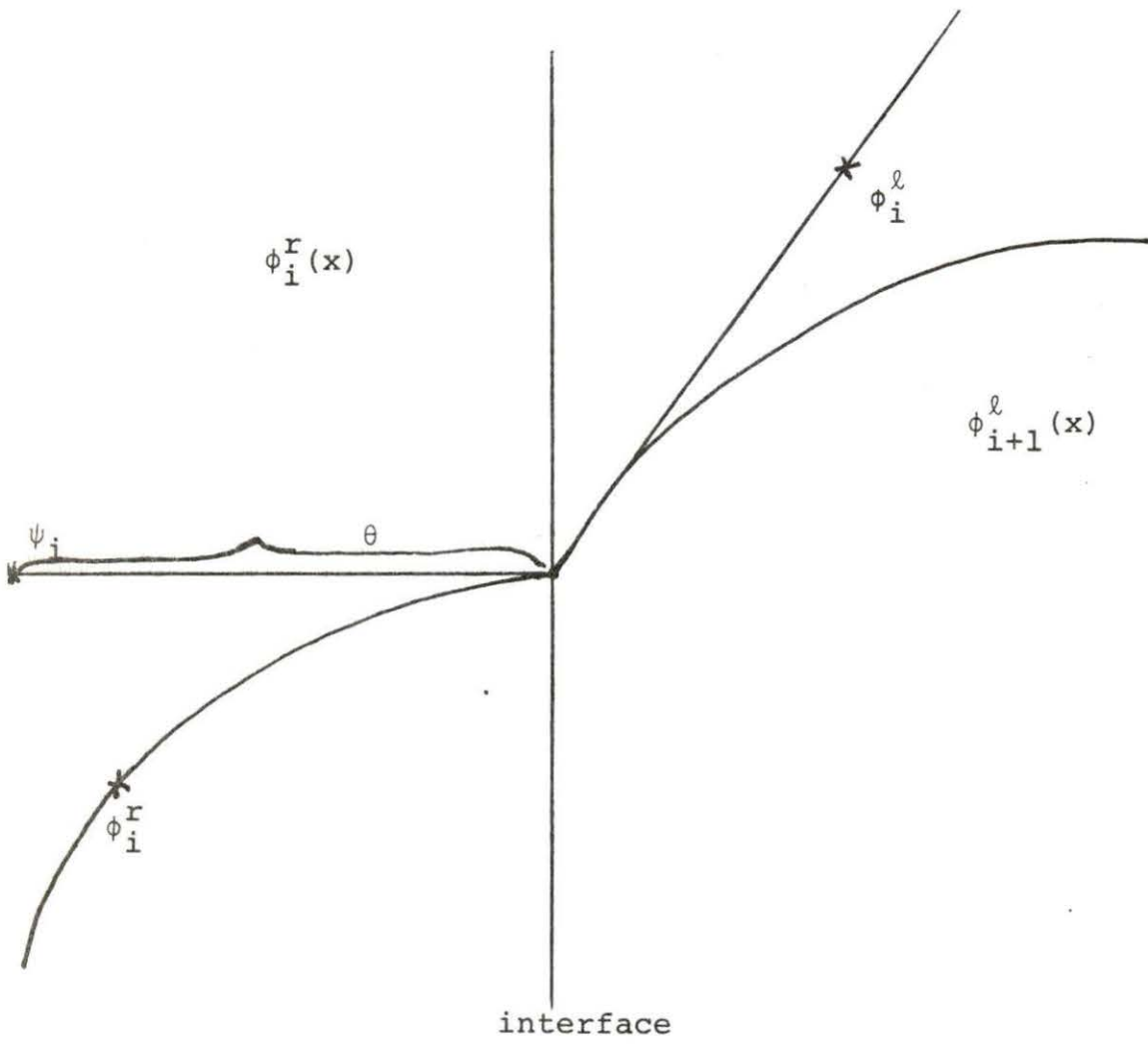Figure 3. Interface flux calculation

node i+1.

Then using the Fick's Law and the continuity of the current, it follows that:

$$D_i \left(\frac{\phi_i^r - \psi_i^r}{\theta} \right) = D_{i+1} \left(\frac{\psi_{i+1}^{\ell} - \phi_{i+1}^{\ell}}{\theta} \right) \quad . \tag{II-28}$$

Hence:

$$\phi_i^r = \frac{D_i \psi_i^r + D_{i+1} \psi_{i+1}^{\ell}}{D_i + D_{i+1}} \quad . \tag{II-29}$$

Then, from equation II-23,

$$\phi_i^r = \phi_{i+1}^{\ell} \quad .$$

e. The albedo calculation   This is also a boundary condition; however, the nodes here are different because it describes the system outer boundary. In this case, the flux at the boundary can be given as an equivalent albedo boundary condition such that:

$$D_I \left. \frac{d\phi(x)}{dx} \right|_{\text{boundary}} = -\tau \phi(x) \bigg|_{\text{boundary}} \tag{II-30}$$

from which one gets:

$$\phi_I^r = - \frac{D_i}{\tau} \left. \frac{d\phi_i}{dx} \right|_{x=n_I} \tag{II-31}$$

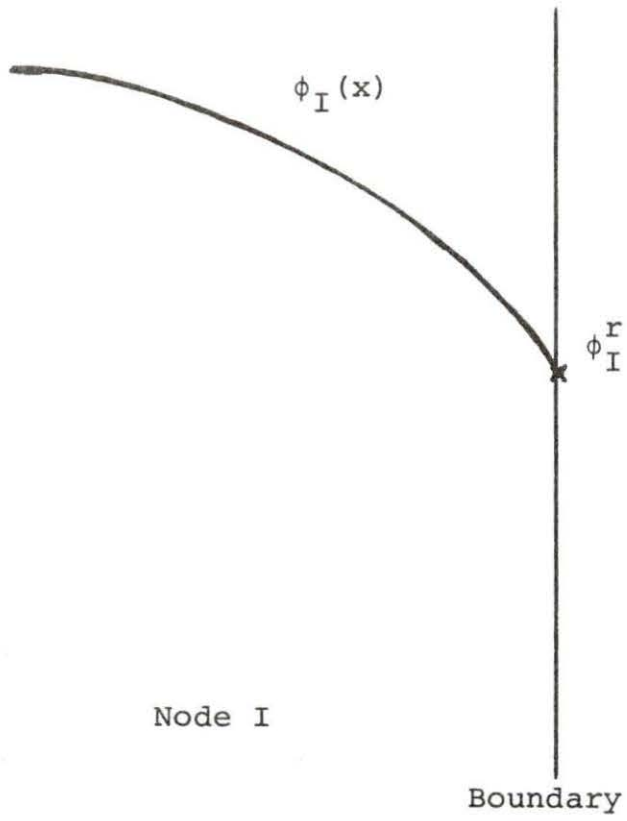where I represents the last fuel assembly (see Fig. 4)

Figure 4. Flux calculation at the outer fuel assembly

and τ is the albedo factor [4].

Using equation II-6, the above equation will give ϕ_I^r in terms of the polynomial coefficients which have been found in the previous iteration.

The basic calculation proceeds as follows:

(1)   Start with an initial flux guess.

(2)   Calculate the polynomial coefficients.

(3)   Calculate the neutron sources.

(4)   Calculate the interface and boundary fluxes.

(5)   Repeat steps 2 to 4 until convergence.

The technique was applied to the "regular configurations" and the results were compared to the two group fine mesh diffusion program called DODMG [5].

Three major points can be noted in the flux shapes:

(1)   The thermal flux peak at the reflector wasn't accurately represented (Fig. 5).

(2)   The flux in the core node next to the reflector was inaccurate (Fig. 5).

(3)   The fast flux was excessively higher in the center half core.

Some attempts were made to solve these discrepancies; unfortunately, the "tilt" in the flux shape didn't vanish (Figs. 7, 8, and 9).

Fig. 7 shows the flux profiles where two nodes per assembly are used in the outer fuel assembly and in the
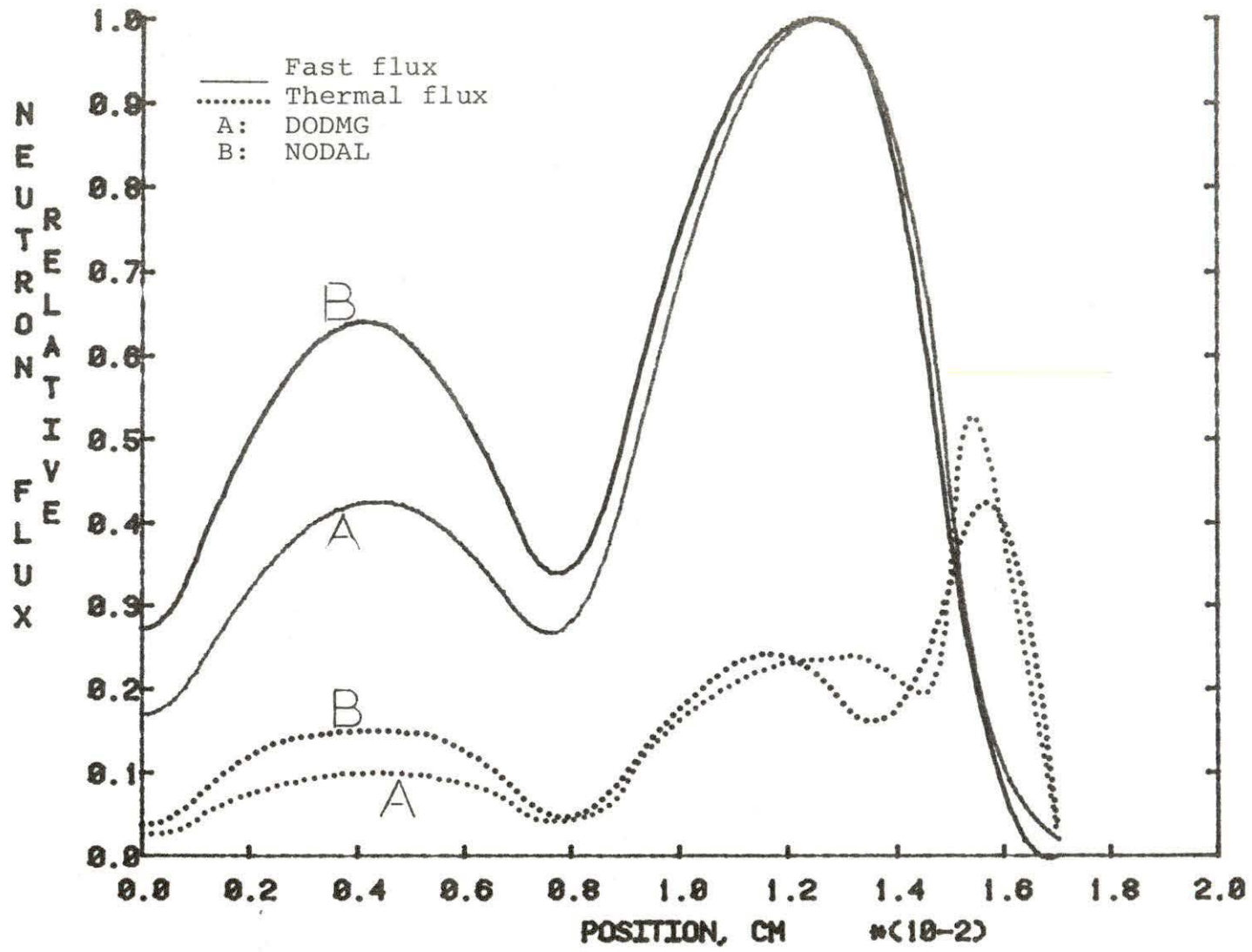
Figure 5. Flux comparison, second order fitting, regular configuration
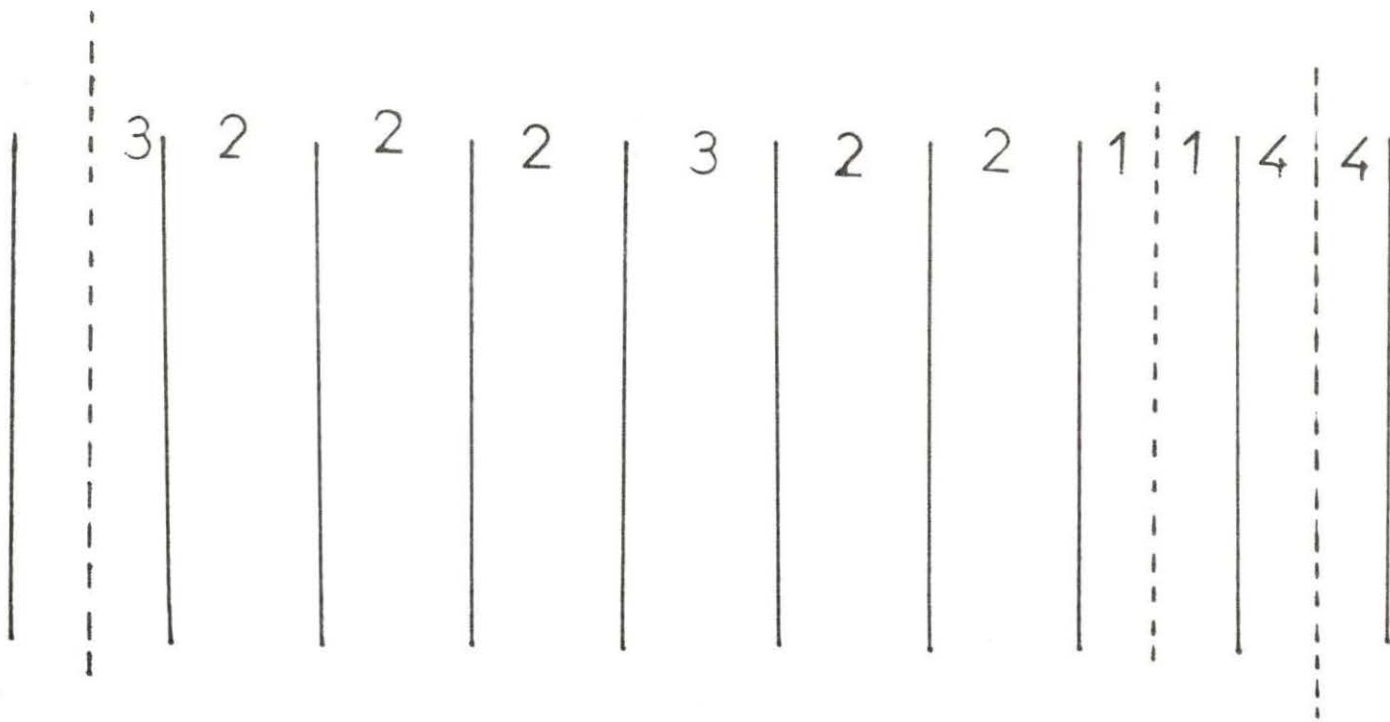
Figure 6. Assemblies arrangement with two nodes per assembly in the outer fuel assembly and in the reflector assembly
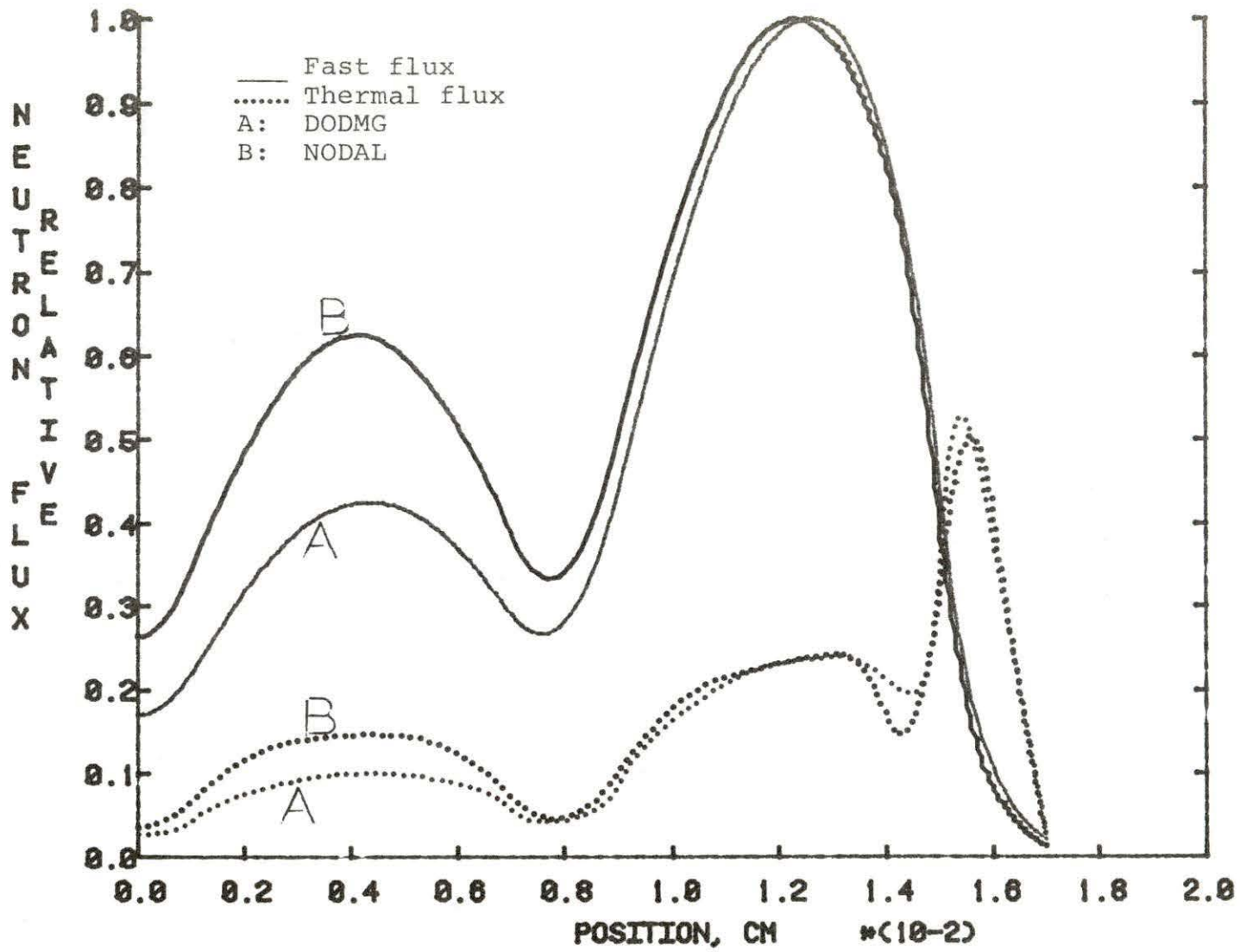
17

Figure 7. Flux comparison, two nodes per assembly in the outer fuel assembly and in the reflector assembly
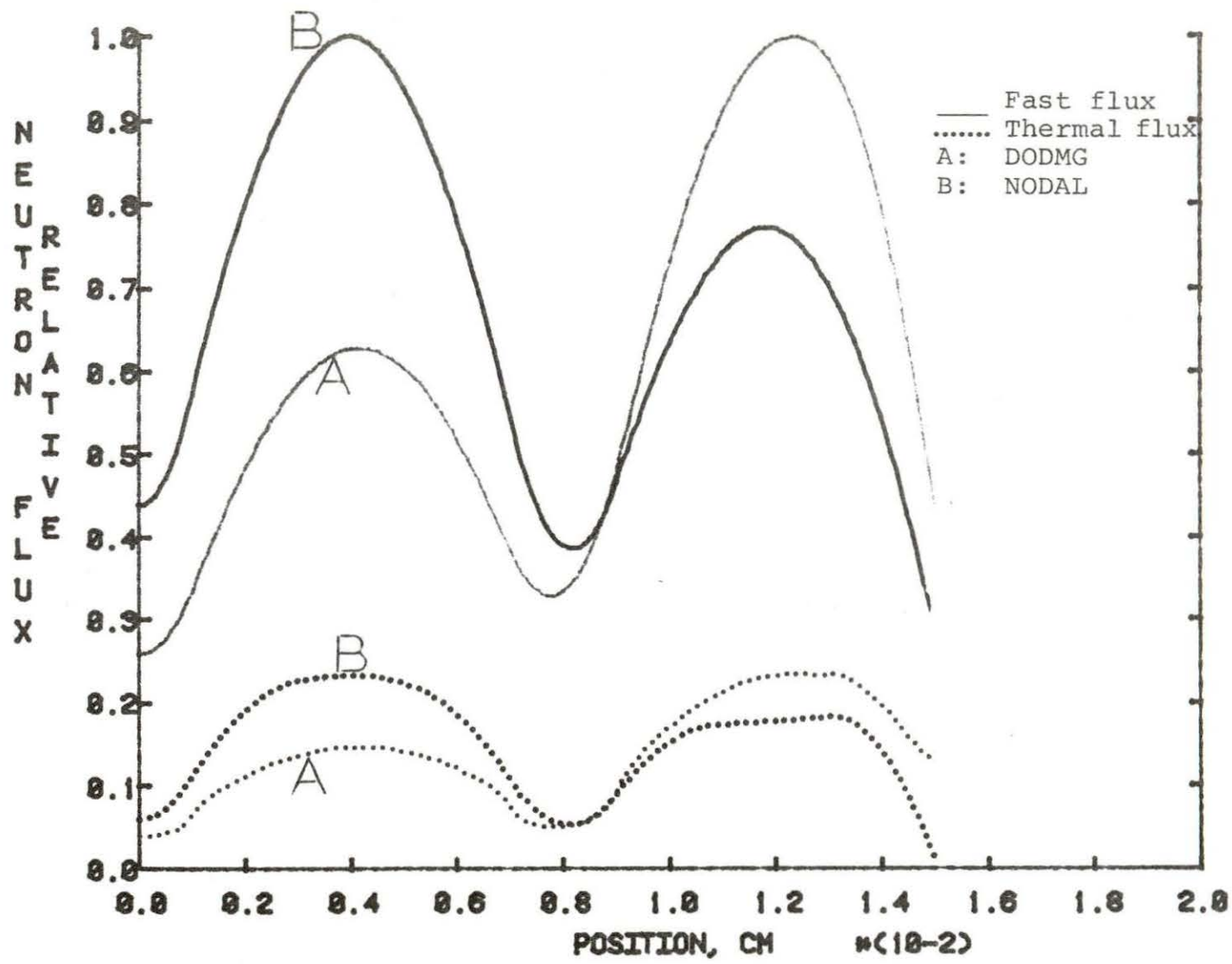
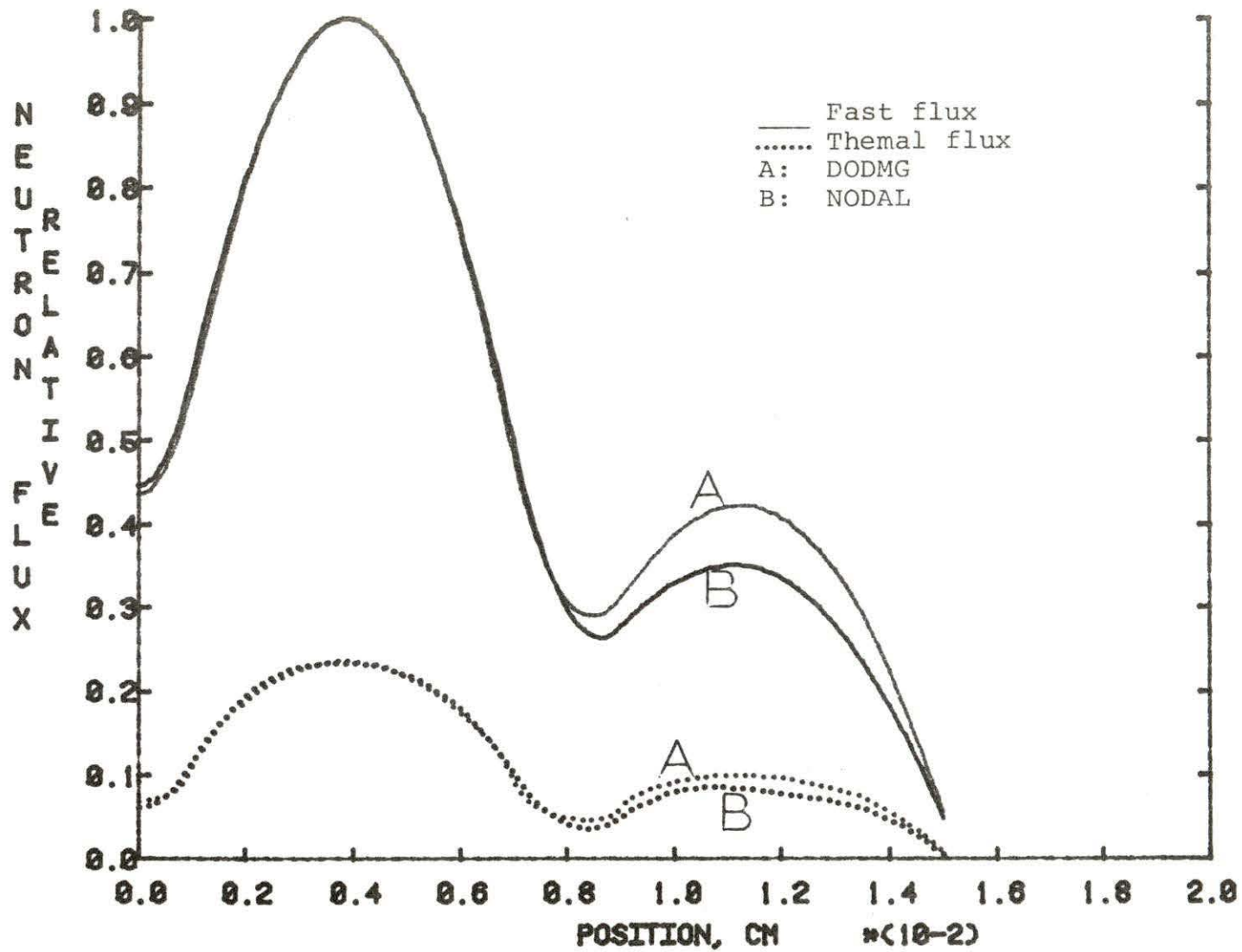Figure 8. Flux comparison, no reflector and albedo condition applied

Figure 9. Flux comparison, no reflector and vacuum boundary condition applied

reflector assembly (see Fig. 6).

Fig. 8 displays the case where the reflector assembly was removed and an arbitrary albedo condition (fast albedo = 0.5 and thermal albedo = 1.0) was applied. In this case, the thermal flux shape at the boundary is "steeper" than it should be. However, this may be expected, since the flux is described by a second order polynomial.

Fig. 9 illustrates the case where the reflector was removed and a vacuum boundary condition applied. The NODAL and DODMG flux profiles are very similar except at the outer nodes.

Finally, an attempt to resolve these errors will be made by the use of a higher order polynomial. This approximation will be used in the remainder of this study.

2. The fourth order fitting

In this case, equations II-6 and II-7 become:

$$\phi_1(x) = a_0 + a_1 x + a_2 x^2 + a_3 x^3 + a_4 x^4 \qquad \text{(II-32)}$$

and

$$\phi_2(x) = b_0 + b_1 x + b_2 x^2 + b_3 x^3 + b_4 x^4 . \qquad \text{(II-33)}$$

Hence, equations II-12 and II-13 become:

$$a_0 = \left(\frac{\phi^\ell + \phi^r}{2}\right) - a_2 \eta^2 - a_4 \eta^4 \qquad \text{(II-34)}$$

and

$$a_1 = \left(\frac{\phi^r - \phi^\ell}{2\eta}\right) - a_3 \eta^2 . \qquad \text{(II-35)}$$

Similarly, equation II-20 will be written as follows:

$$a_2 = -\frac{1}{2}(\alpha_1 \tilde{a}_0 + \alpha_2 \tilde{b}_0) - \frac{\eta^2}{6}(\alpha_1 \tilde{a}_2 + \alpha_2 \tilde{b}_2)$$
$$-\frac{\eta^4}{10}(\alpha_1 \tilde{a}_4 + \alpha_2 \tilde{b}_4) - a_4 \eta^2 . \qquad \text{(II-36)}$$

Finally, using the minimization technique with respect to a_3 and a_4, we get:

$$a_3 = -\frac{1}{6}(\alpha_1 \tilde{a}_1 + \alpha_2 \tilde{b}_1) - \frac{\eta^2}{10}(\alpha_1 \tilde{a}_3 + \alpha_2 \tilde{b}_3) \qquad \text{(II-37)}$$

and

$$a_4 = -\frac{1}{12}(\alpha_1 \tilde{a}_1 + \alpha_2 \tilde{b}_2) - \frac{\eta^2}{14}(\alpha_1 \tilde{a}_4 + \alpha_2 \tilde{b}_4) . \qquad \text{(II-38)}$$

Therefore, the problem at present will be to solve equations II-34 through II-38 with the source and interface conditions, the same as described previously.

III. THE COMPUTATIONAL PROCEDURE

The equations obtained above can only be solved by some iterative technique; the relaxation method was selected. This technique has already demonstrated its effectiveness with the nodal model, especially when a suitable accelerating technique is applied.

At this stage, two fundamental definitions must be introduced; they will be frequently used.

A. Fundamental Definitions

1. Definition (1) [2]

A sequence

$$\{\underline{x}^k\}_{k=1}^{\alpha}$$

of vectors in R^n is said to converge to x with respect to the norm $\|.\|$ if given any $\varepsilon > 0$ there exists an integer $N(\varepsilon)$ such that:

$$\|\underline{x}^{(k)} - \underline{x}\| \leq \varepsilon, \text{ for all } k \geq N(\varepsilon) \quad . \quad \text{(III-1)}$$

Since all norms on R^n are equivalent with respect to convergence [2], the Euclidian norm will be used.

2. Definition (2) [6]

The residual vector is defined as follows:

$$\underline{r}^{\ell} = \underline{x}^{(\ell+1)} - \underline{x}^{(\ell)} \quad . \quad \text{(III-2)}$$

In our problem, $\underline{x}$ will represent any of the coefficients, the average flux or the source expressions. In terms of the errors, equation III-1 becomes:

$$\underline{r}^\ell = \underline{\varepsilon}^{(\ell+1)} - \underline{\varepsilon}^{(\ell)} \qquad \text{(III-3)}$$

where ε^ℓ is the error at iteration (ℓ) and $\varepsilon^{(\ell+1)}$ is the error at the following iteration.

Then, using the stability condition [5], we define the rate of convergence v as:

$$v = - \ln \lambda_1 \qquad \text{(III-4)}$$

where λ_1 = largest eigenvalue of the iteration matrix.

The λ_1 can be approximated by using the ratio of two successive residual vectors, that is:

$$\lambda_1 = \frac{|\underline{r}^{\ell+1}|}{|\underline{r}^\ell|} \qquad . \qquad \text{(III-5)}$$

Hence, one can write:

$$v = - \ln \frac{|\underline{r}^{\ell+1}|}{|\underline{r}^\ell|} \qquad . \qquad \text{(III-6)}$$

Furthermore, the residual vector for the average flux will be:

$$\underline{r}^\ell = \frac{\overline{\phi}^{(\ell+1)} - \overline{\phi}^{(\ell)}}{\overline{\phi}^\ell} \qquad . \qquad \text{(III-7)}$$

Then, using equation III-1, we define the SNORM as:

$$\text{SNORM} = \frac{\sqrt{\sum_i \left(1 - \frac{\bar{\phi}^\ell}{\bar{\phi}^{\ell+1}}\right)^2}}{\text{IMAX}} \leq \varepsilon \tag{III-8}$$

where IMAX = total number of nodes.

From equation III-6, we note that for a preset ε, the smaller the slope of the SNORM, the faster the convergence will be.

Hence, the SNORM versus number of iteration plots will be extensively used to describe the convergence of the system.

B. The Relaxation Method (RM)

The general form of the iterative process is given by:

$$x^{(\ell+1)} = x^{cal}\alpha + (1-\alpha)x^{(\ell)} \tag{III-9}$$

where x^{cal} = the value of x calculated using the Seidel method. Here, it will be calculated by the analytical expressions of the unknowns such as equations II-35 to II-39).

α = Relaxation parameter.

x^ℓ = The value of x from the previous iteration.

A major problem associated with the use of the RM is the determination of the optimal relaxation factors.

C. The Accelerating Technique

1. Introduction

There are several accelerating techniques that one can apply to hasten the convergence of a slowly convergent problem. These techniques vary from a simple extrapolation to some sophisticated matrix manipulation [7].

However, the equations we are solving are strongly coupled (see equations II-35 to II-39); therefore, the iterative matrix isn't easy to write. Hence, the usual routines to find α_{op} may not be used, so special techniques are needed.

2. The experimental method [6, 8]

This technique consists of carrying out several iterations with various α values ($1 \leq \alpha < 2$) and observing the number of iterations for convergence. The α yielding the minimum number of iterations is chosen as α_{op}. Instead of the number of iterations, one can use the spectral radius of the matrix. For this case, the α_{op} will correspond to the least absolute value of the largest eigenvalue of the system [8].

IV. RESULTS

A. Application of the Technique to the Regular Configuration

The overall flowchart is shown in Fig. 10. As described in section II-C, the computation starts with some initial guess of the coefficients and fluxes. Then, the coefficients are calculated using equations II-35 to II-39. To insure the continuity of the fluxes, the interface and albedo conditions are applied; then new fluxes and source are calculated. The iterations continue until the flux changes are less than a preset tolerance criterion.

1. General behavior of the relaxation parameters

In this problem, seven relaxation parameters were used. These include the five polynomial coefficients, the source term, and the interface values. They will be called α_{c_i} for $i=0,\ldots,4$, α_s and α_{in}, respectively.

The following remarks helped the author simplify considerably the computation:

(1) The coupling among the unknowns a_2, a_3 and a_4 suggests that the corresponding relaxation parameters must be underrelaxed in order to reduce the effect of the coupling on the convergence. Moreover, α_{c_3} and α_{c_4} may be kept equal to α_{c_2} which monitors the flux shape (see second order
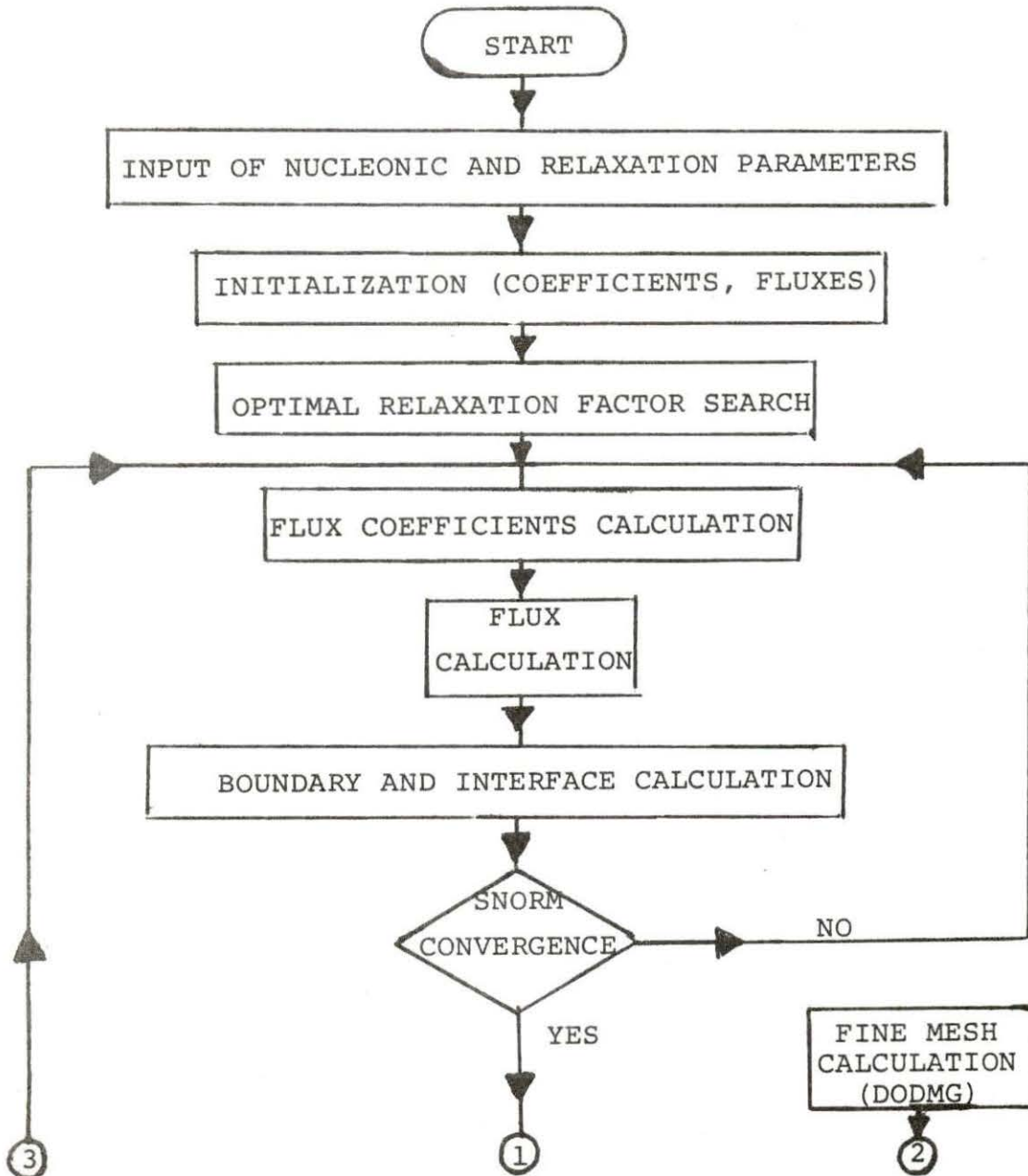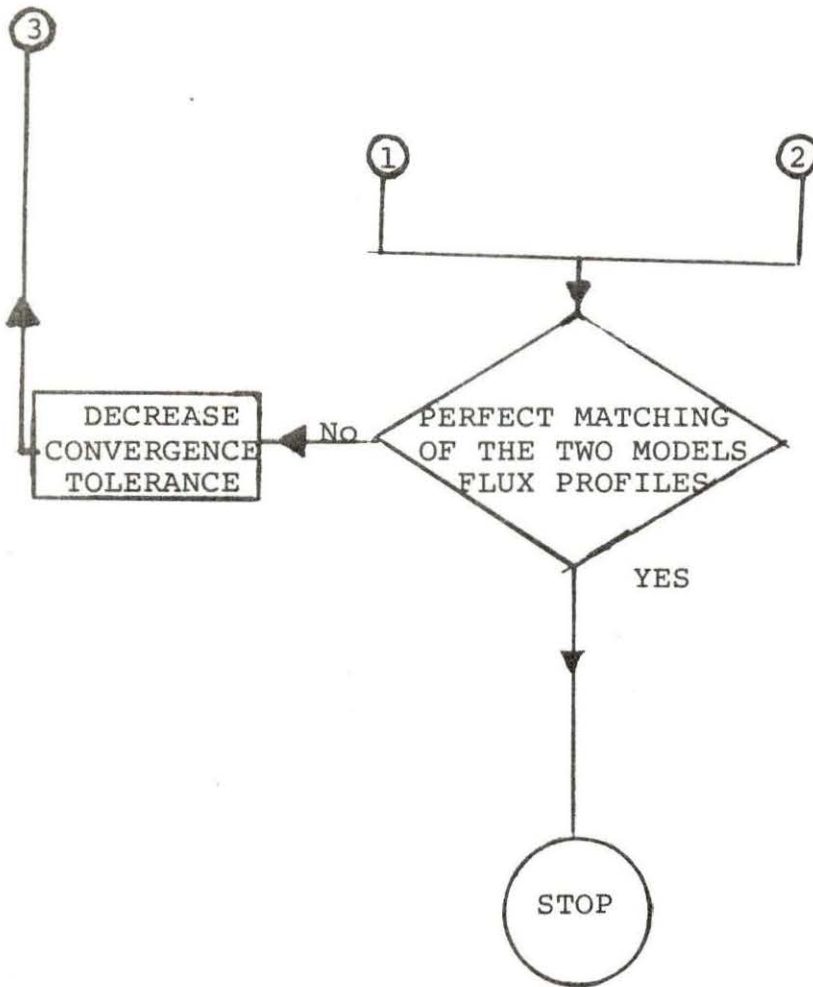
Figure 10.   Problem analysis flow chart

Figure 10.   (Continued)

fitting results).

(2) On the other hand, previous studies [7] show
that the relaxation factor α_{in} should also be
underrelaxed.

(3) Concerning α_{c_0} and α_{c_1}, they will be kept equal to
unity, since their effects are already considered
in the expression of a_2 and a_4, and a_3, respec-
tively.

Therefore, one can reduce the optimization problem
to that of only three parameters, α_s, α_{in} and α_{c_2}.

2. Determination of the optimal relaxation parameters

Before the accelerating technique was applied, one
needed to insure the problem convergence. This was done
by using the trial and error process on the relaxation
factors. We found that the system converged for the follow-
ing parameters:

$$\alpha_{c_0} = \alpha_{c_1} = 1.0$$

$$\alpha_{c_2} = \alpha_{c_3} = \alpha_{c_4} = 0.05$$

$\alpha_s = 1.3$ and $\alpha_{in} = 1.0$, the tolerance ε was 10E-4.

Then, as for the second order expansion, the results
were compared to the DODMG solution. Figs. 11-13 illustrate
the fluxes, the SNORM and the eigenvalue profiles obtained
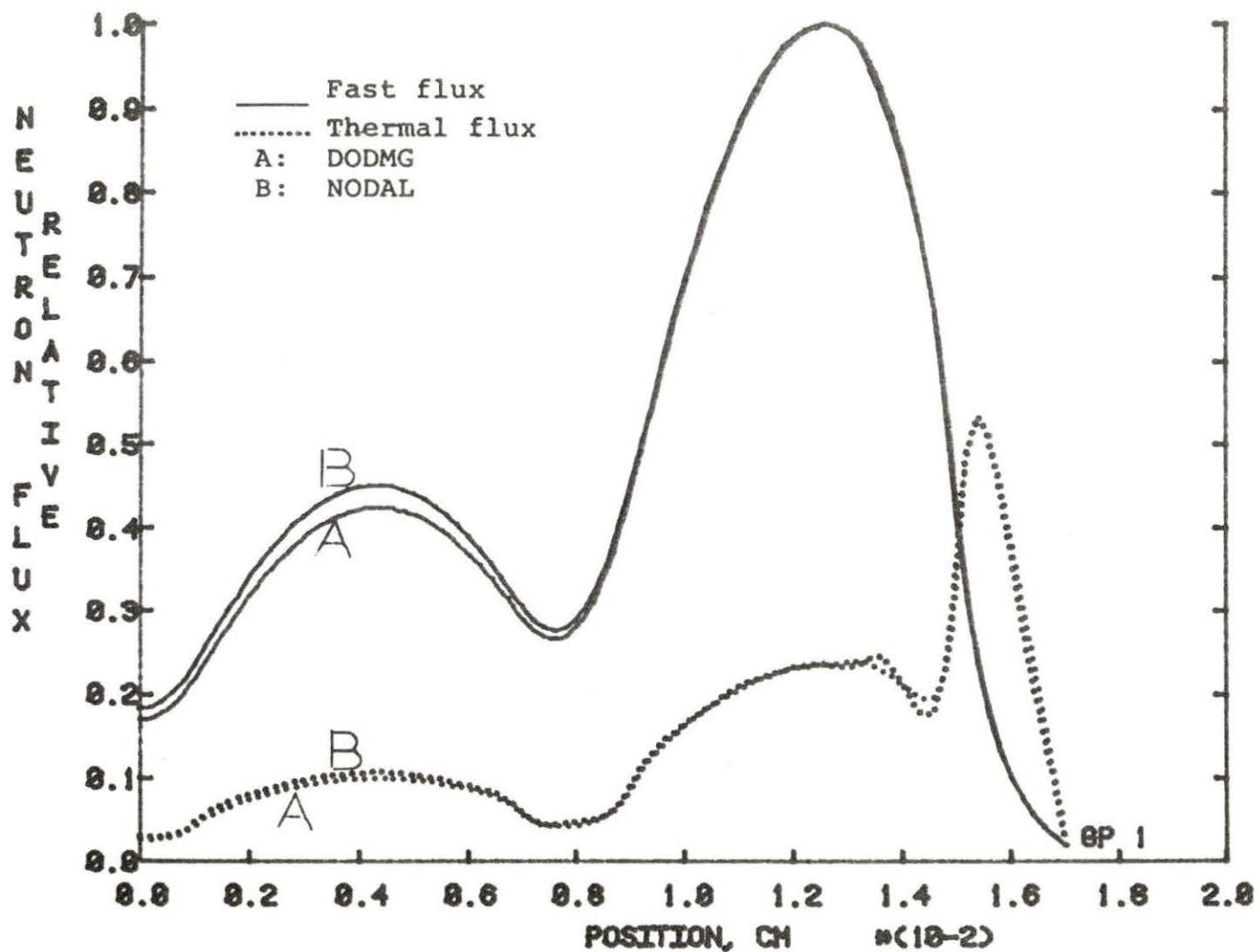
Figure 11. Flux profiles comparison for original relaxation parameters
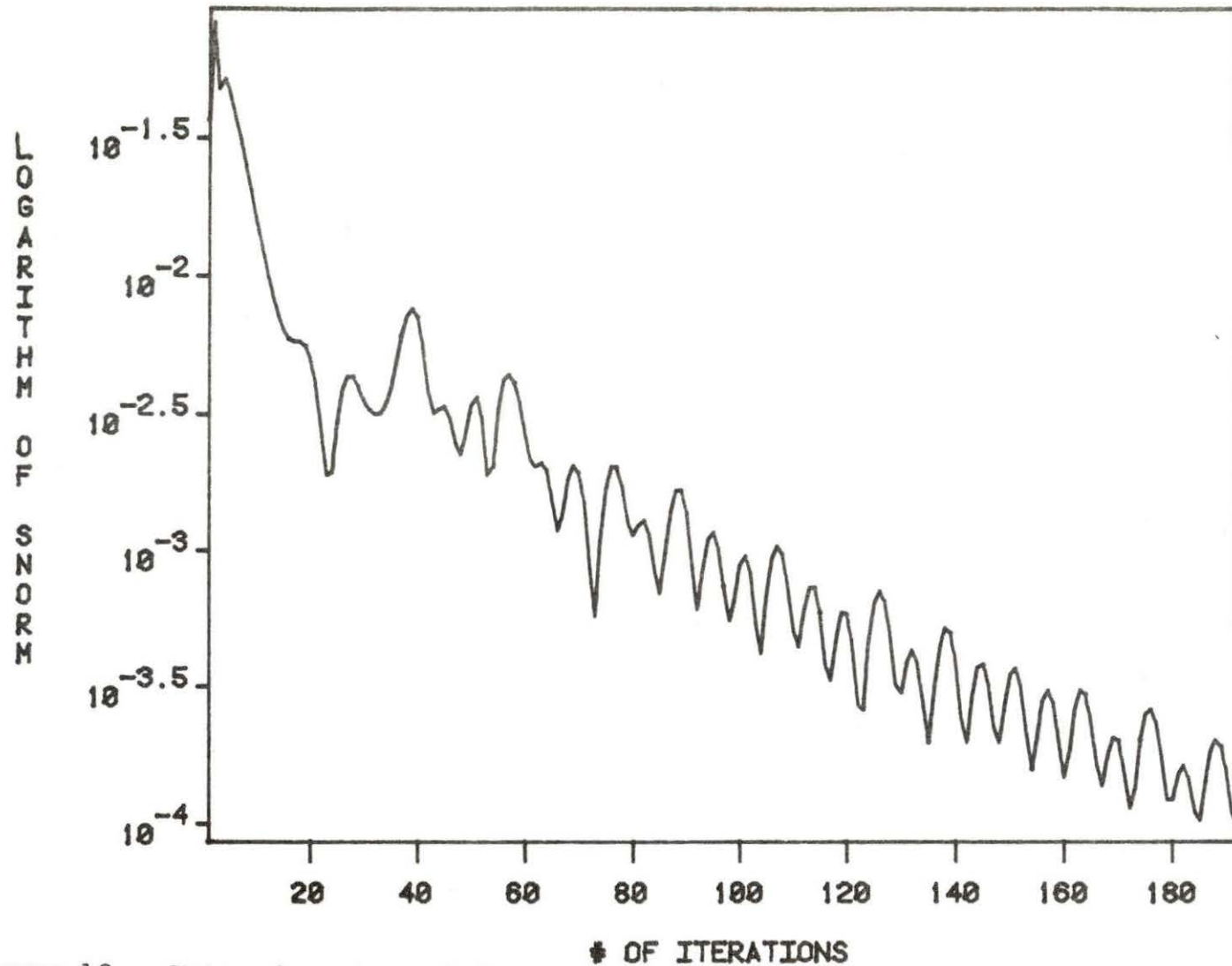
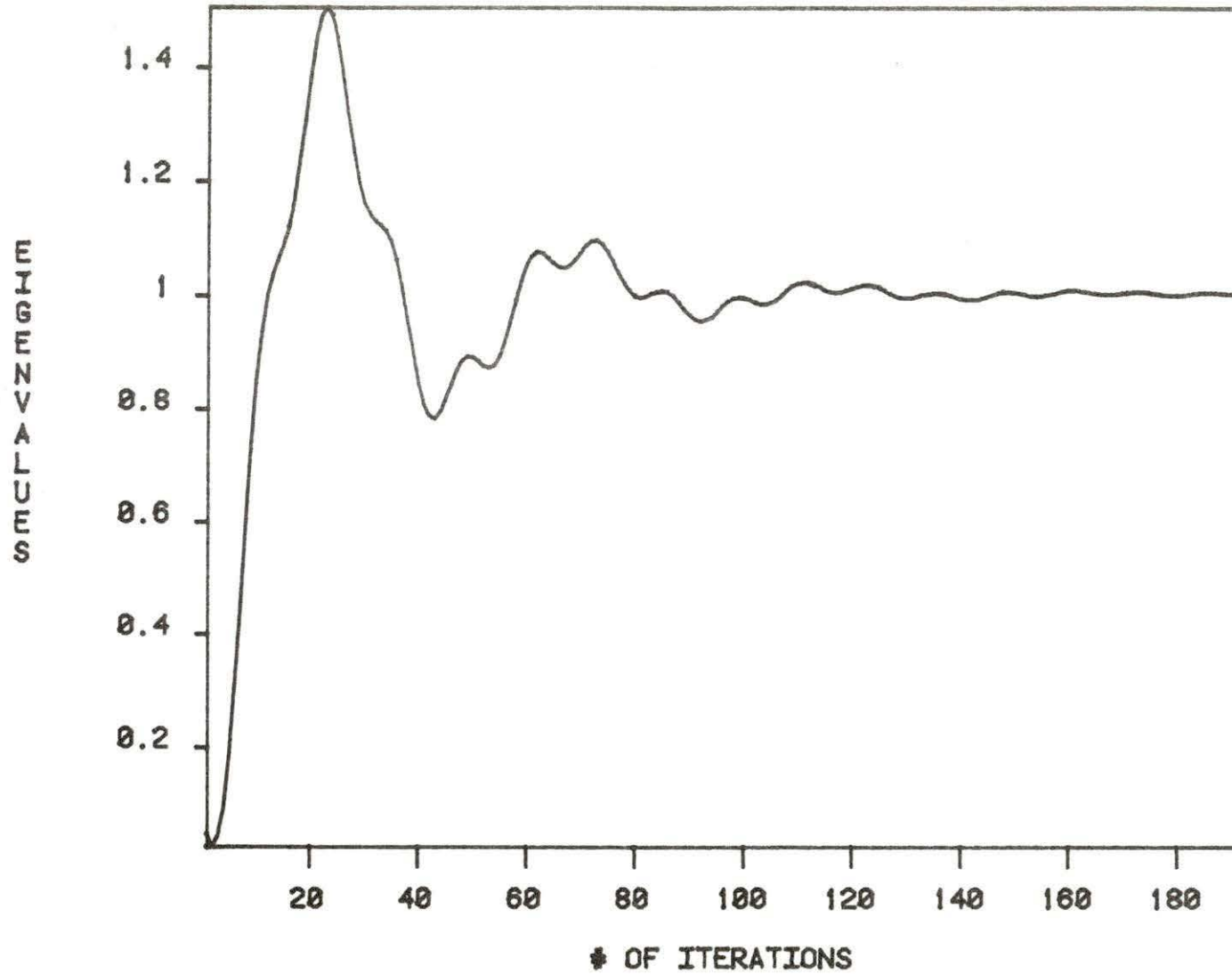Figure 12.   SNORM for the original relaxation parameters

Figure 13. Eigenvalue convergence for the initial relaxation parameters

for the above data.

From these plots, we note that the SNORM curve shows some continuous oscillations which characterize the instability of the solution. Moreover, the flux profiles show a large deviation from the fine mesh fluxes.

An attempt to solve these discrepancies was to decrease the tolerance to 10E-7. Unfortunately, this didn't resolve the error, as is seen in Figs. 14-16. Therefore, the experimental method was considered and first applied to α_{c_2}. The relaxation factors α_s and α_{in} were kept equal to their original values (1.3 and 1.0, respectively) and α_{c_2} was given different values between 0.0 and 1.0. The least number of iterations needed for the SNORM to reach 10E-4 was recorded. Fig. 17 shows the α_{c_2} versus number of iterations. One can note that several α_{c_2} values correspond to the minimal number of iterations which is 72. The situation is even worse for α_s and α_{in} plots (see Figs. 18 and 19). Therefore, the experimental technique needed to be improved. The SNORM was used for this purpose. Hence, from all the relaxation factors corresponding to the least number of iterations, the one which gave the smallest SNORM was selected as the α_{op}. Tables 2, 3 and 4 list some α values and their respective SNORMs. The following optimal relaxation factors were then obtained:
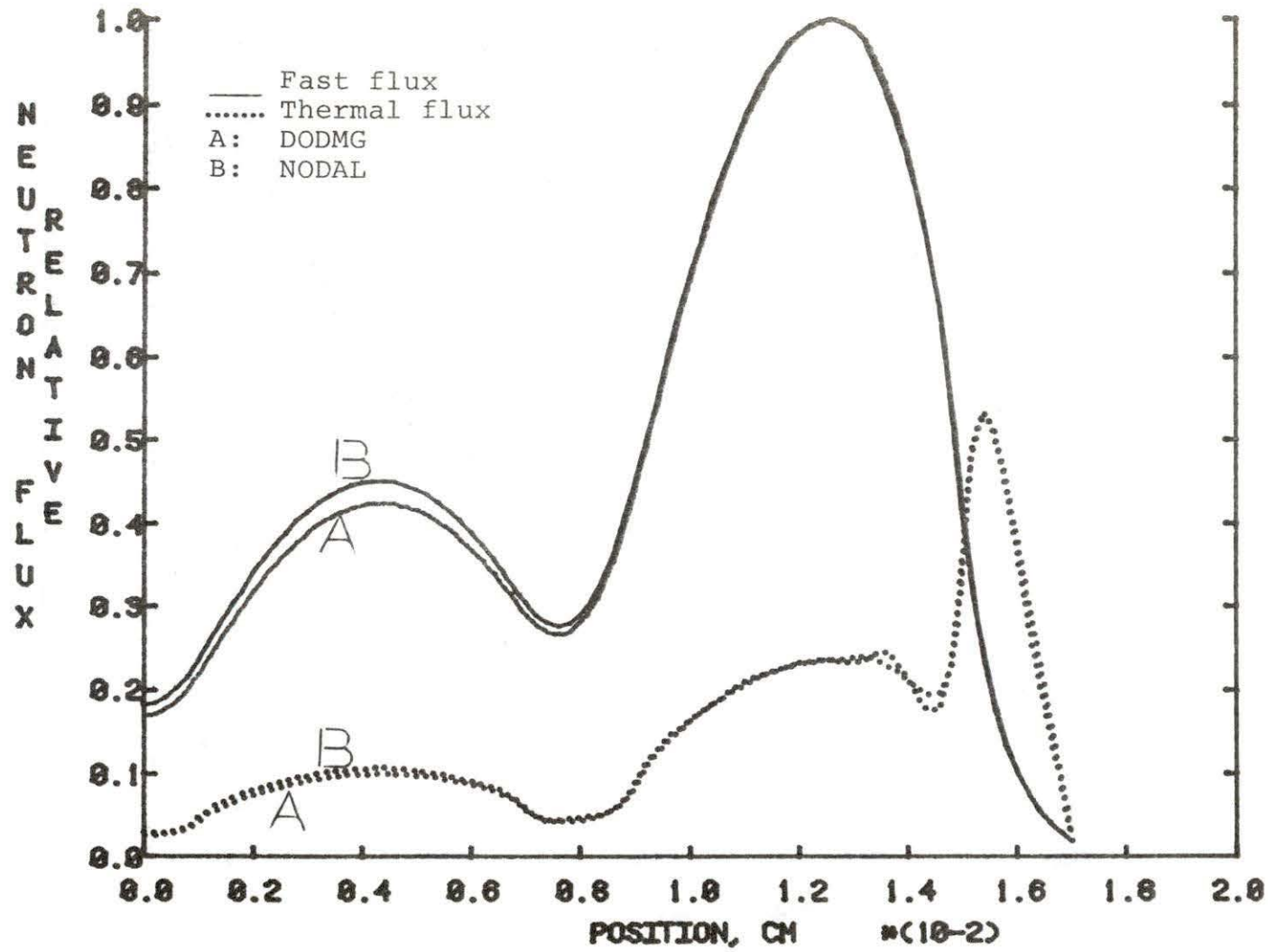
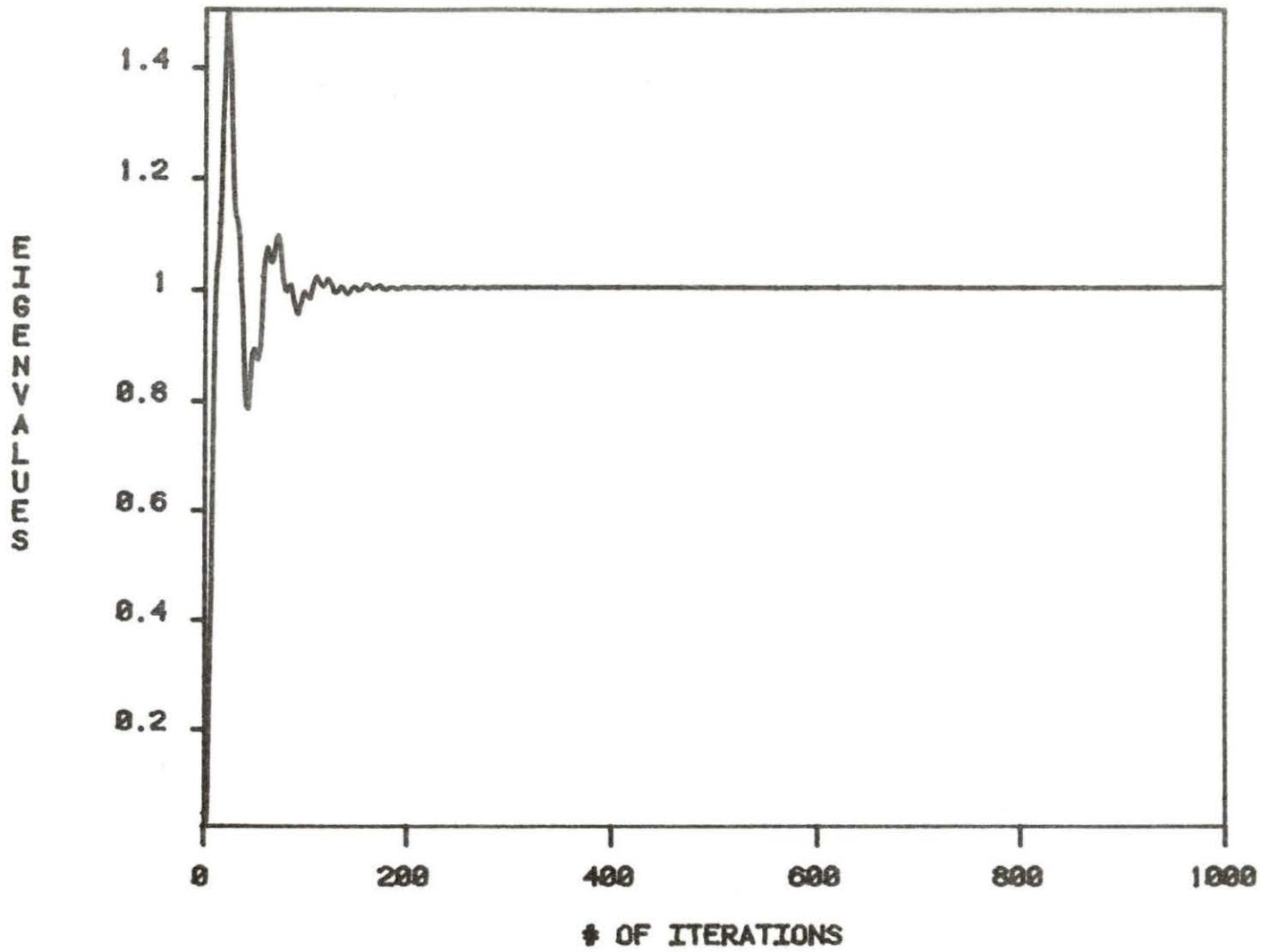Figure 14. Flux shape comparison for the initial relaxation parameters

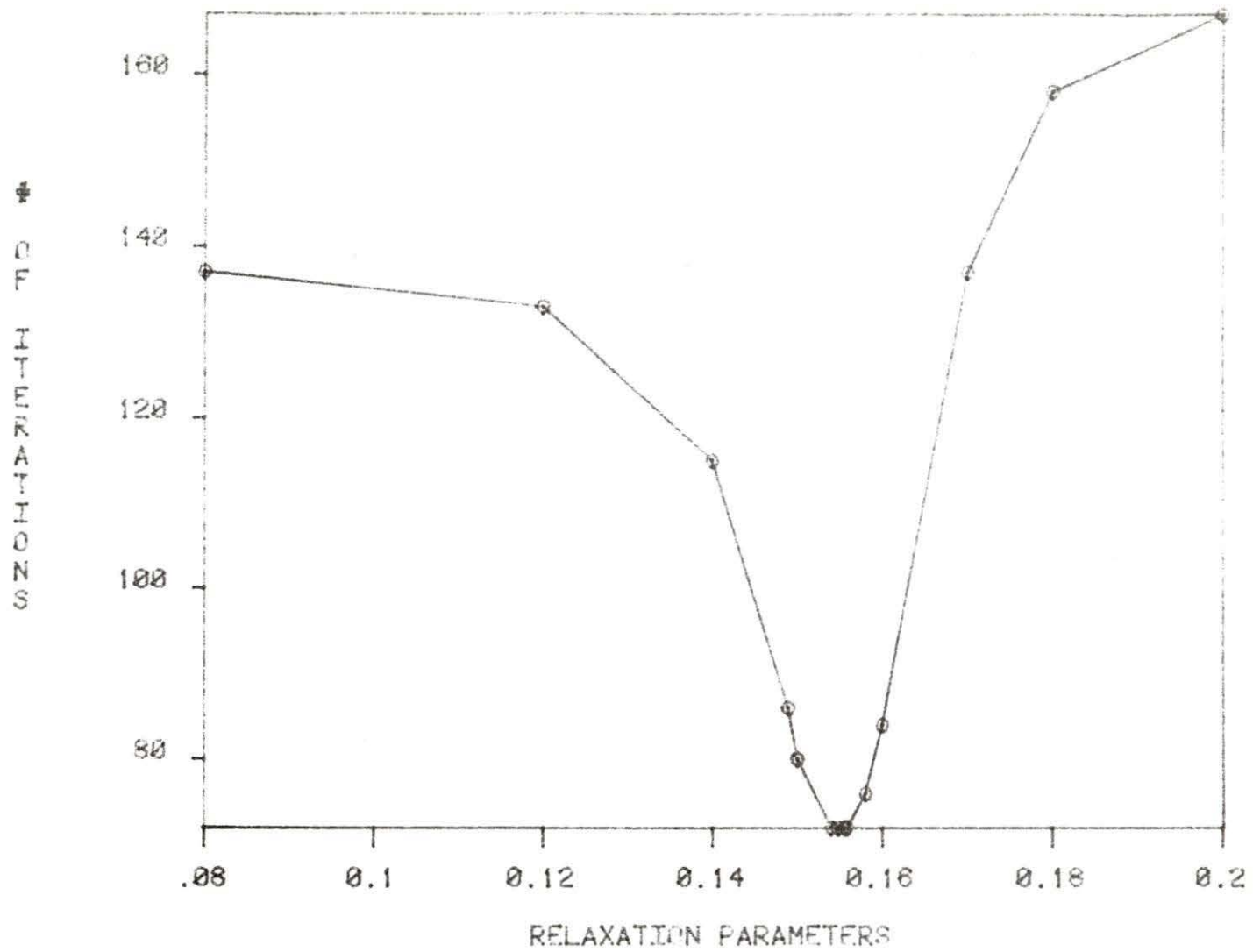Figure 16.   Eigenvalue convergence for original relaxation parameters
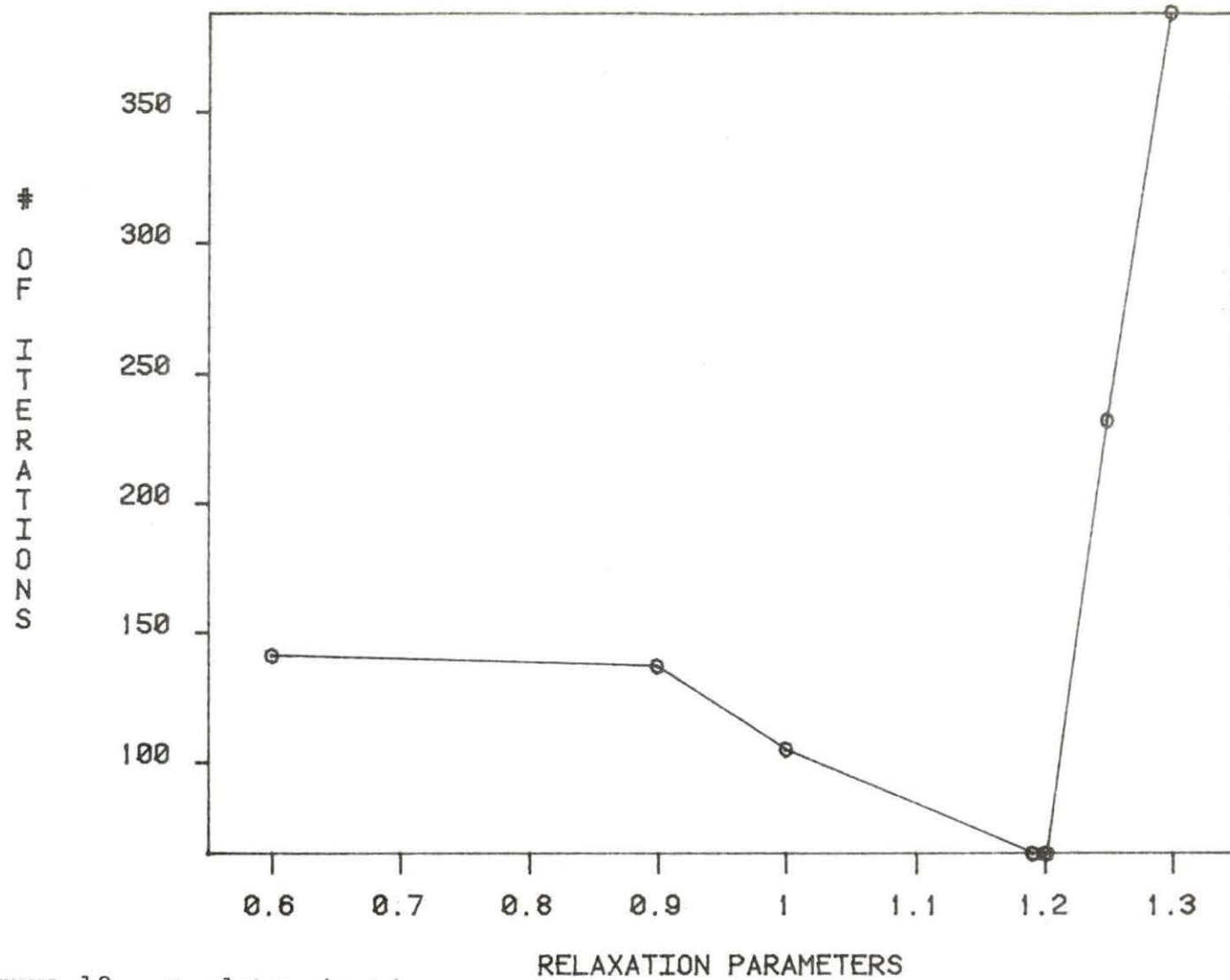
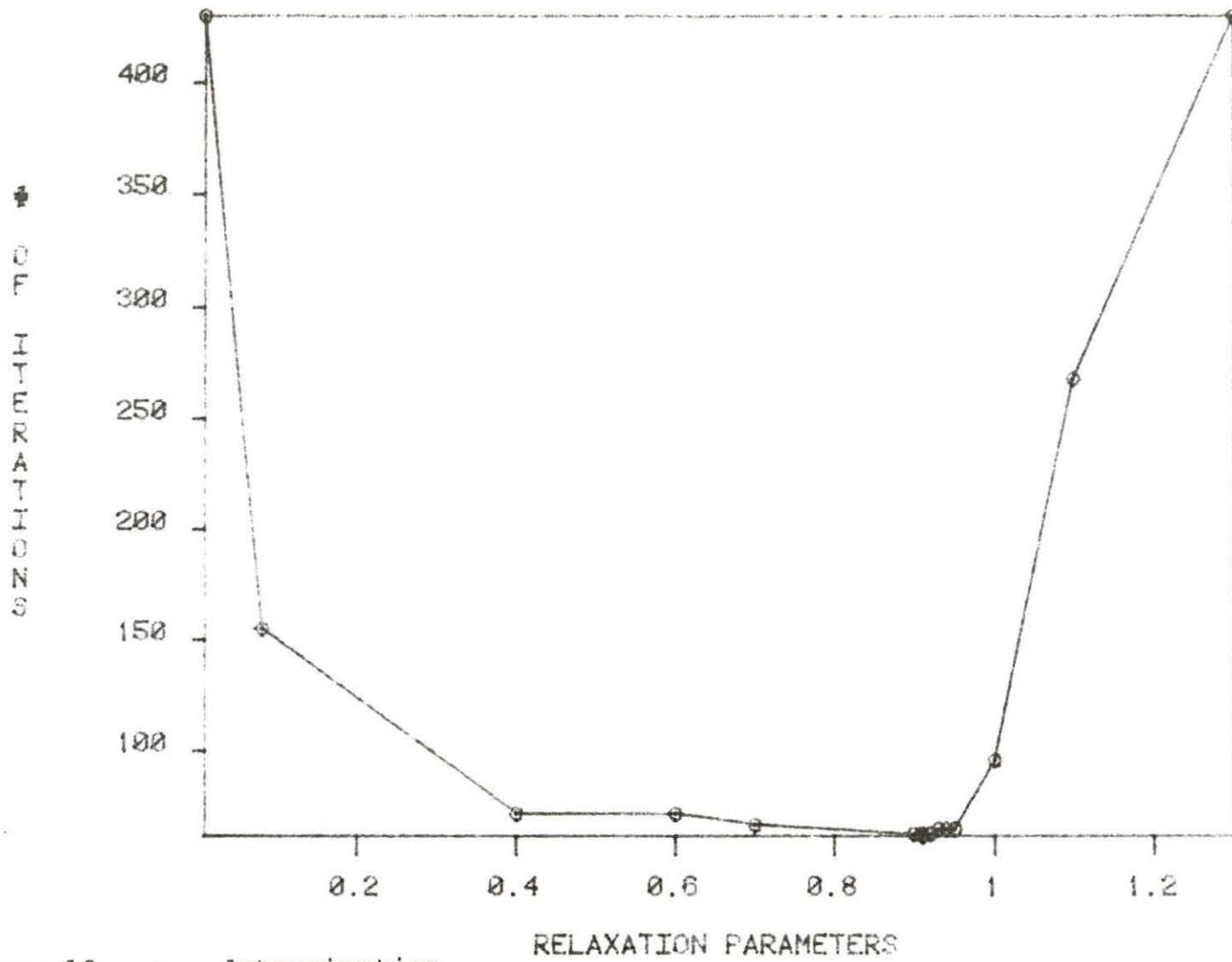Figure 17. α_{c_2} determination

Figure 18. α_s determination

Figure 19. α_{in} determination

Table 2. α_{c2} values and the respective SNORM at 72 iterations

α_{c2}	0.154	0.1549	0.1545[a]	0.1547	0.155	0.1555
Error (10^5)	9.877	9.871	9.864	9.866	9.875	9.922

[a]Selected value.

Table 3. α_{in} values and the respective SNORM at 65 iterations

α_{in}	0.9	0.92	0.945	0.95
Error (10^5)	9.454	9.5011	8.1764	7.99
α_{in}	0.9502	0.9504	0.9508[a]	0.96
Error (10^5)	7.986	7.980	7.9708	8.211

[a]Selected value.

Table 4. α_s values and the respective SNORM at 65 iterations

α_s	1.1902	1.1908	1.2[a]	1.202
Error (10^5)	8.1022	8.07	7.97	8.050

[a]Selected value.

$$\alpha_{c_2} = \alpha_{c_3} = \alpha_{c_4} = 0.1545$$

$$\alpha_s = 1.200$$

$$\alpha_{in} = 0.9508 \quad .$$

Since the technique was applied to each parameter separately, the values obtained may not be the optimal factors for the global problem. However, their feasibility was checked by seeking the α_{op} in an opposite sequence, that is, keeping α_{c_2} and α_s at their original values (0.05 and 1.3, respectively) and varying α_{in}. The same results were obtained.

For the above factors, the program was run and the results are recorded in Figs. 20-22.

Fig. 20 represents the flux profile comparison with DODMG. An excellent matching can be observed. Moreover, the SNORM (Fig. 21) oscillated to a lesser degree but decreased continuously. In the eigenvalue plot (Fig. 22), one can see that the k_{eff} reached a constant value after 45 iterations.

B. Application of the Technique to Other Problems

The credibility of the determined parameters was tested using different problems. They will be discussed in the following sections.
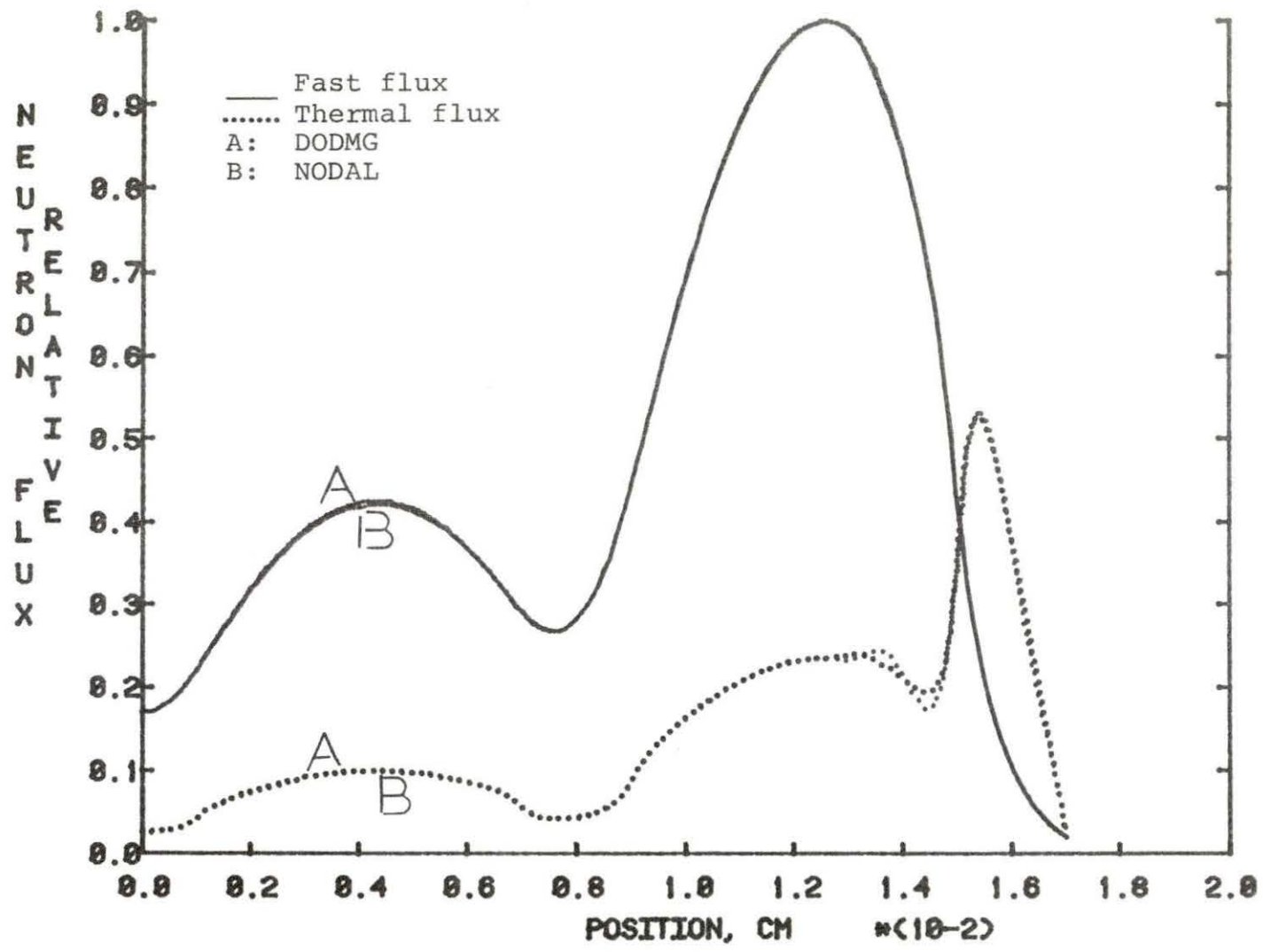
Figure 20. Flux profiles comparison (optimal relaxation factors)
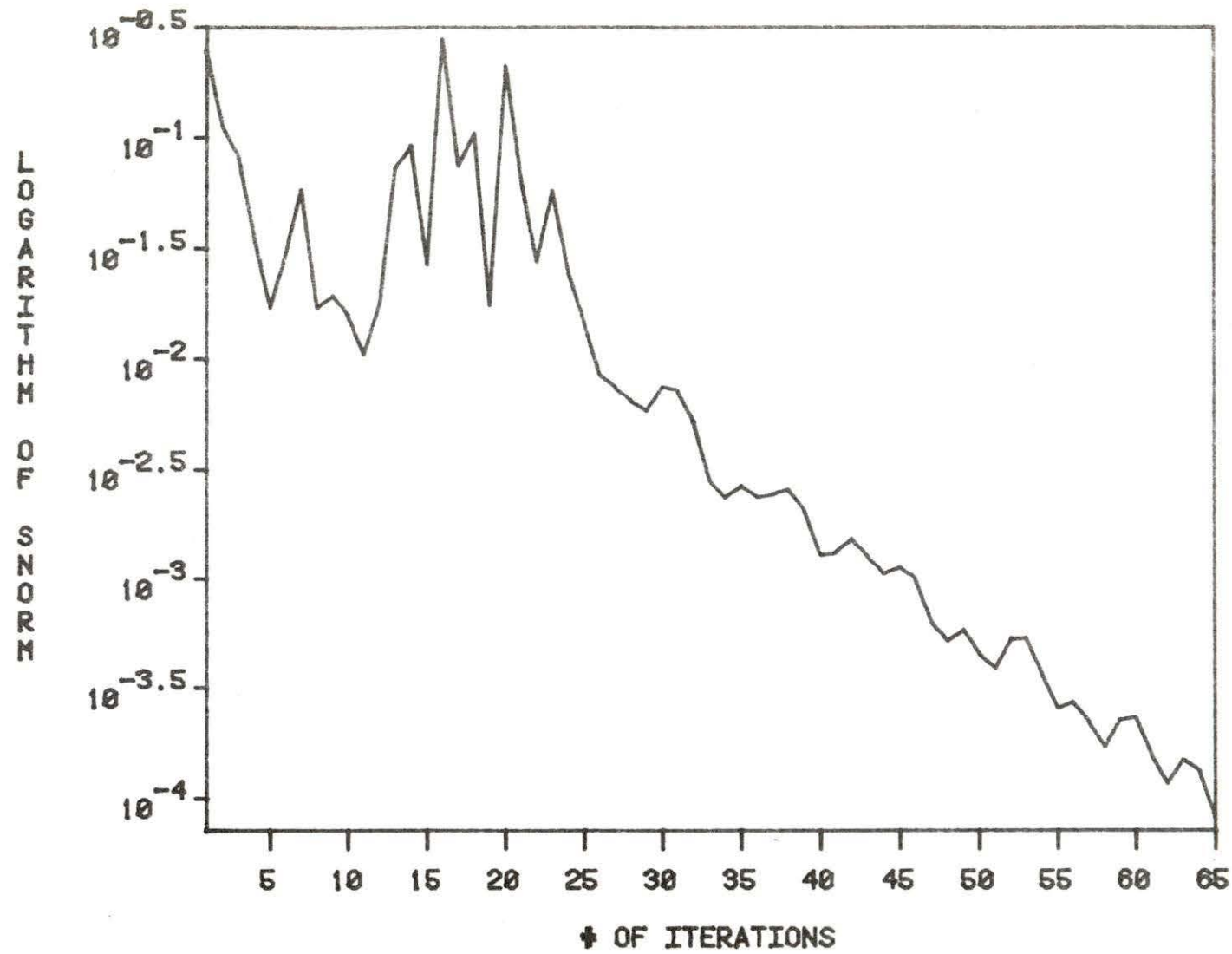
Figure 21.   SNORM versus number of iterations for optimal relaxation factors
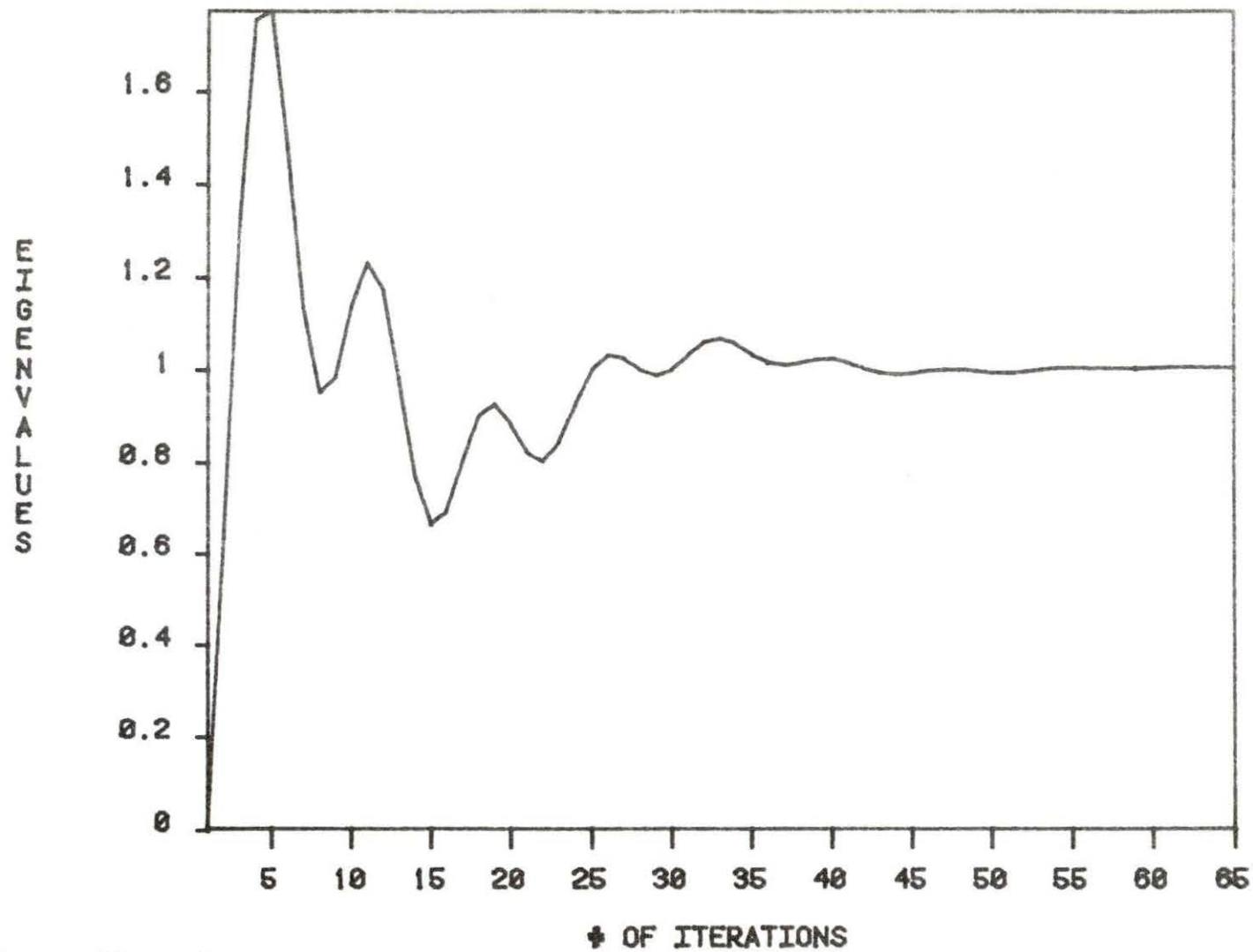
Figure 22.   Eigenvalues for optimal relaxation factors

1. Regular configuration with two
   assemblies shuffled

   The assemblies' disposition is illustrated in Fig. 23.
This may be the case in a fuel management problem.

2. Regular configuration without
   reflector

   In the regular configuration, the reflector was re-
moved. Even though this is not a realistic situation, one
can judge better the polynomial expansion since an important
flux variation is expected.

3. Configuration with burnable poison

   In this case, the fuel assemblies are alternated with
burnable poison assemblies. Fig. 24 shows the node arrange-
ment. The fuel parameters for this problem are listed in
Table 5. Note also that the thermal albedo was increased
to unity.

Table 5. Burnable poison and fuel parameters

Fuel type	D_1	D_2	$\Sigma_{1 \to 2}$	Σ_{a_1}	Σ_{a_2}	$\nu\Sigma_{f_2}$	$\nu\Sigma_{f_1}$
3	1.2475	0.3775	1.7476E-2	9.193E-3	8.556E-2	0.1160	6.027E-3
5	1.2315	0.3801	1.7506E-2	9.276E-3	7.896E-2	0.1233	6.436E-3
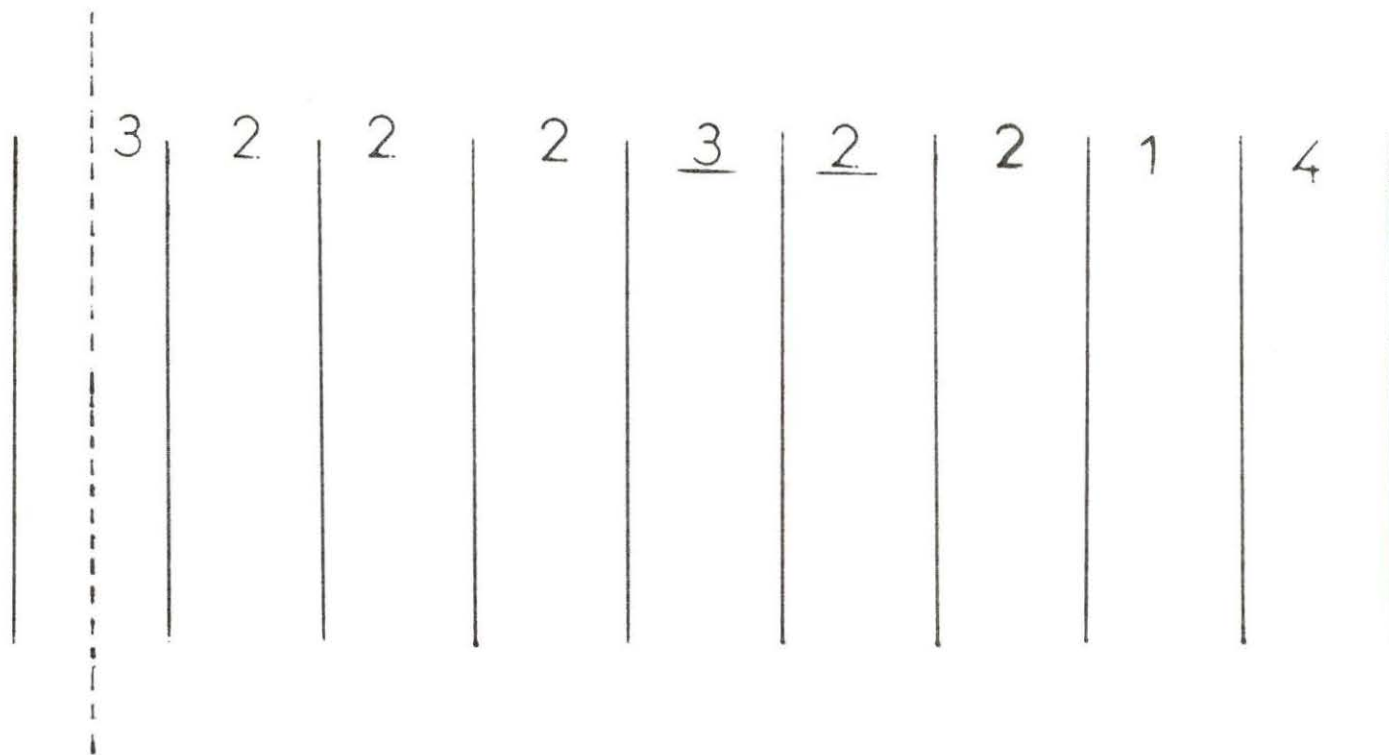
Figure 23. Assemblies arrangement showing the two shuffled assemblies
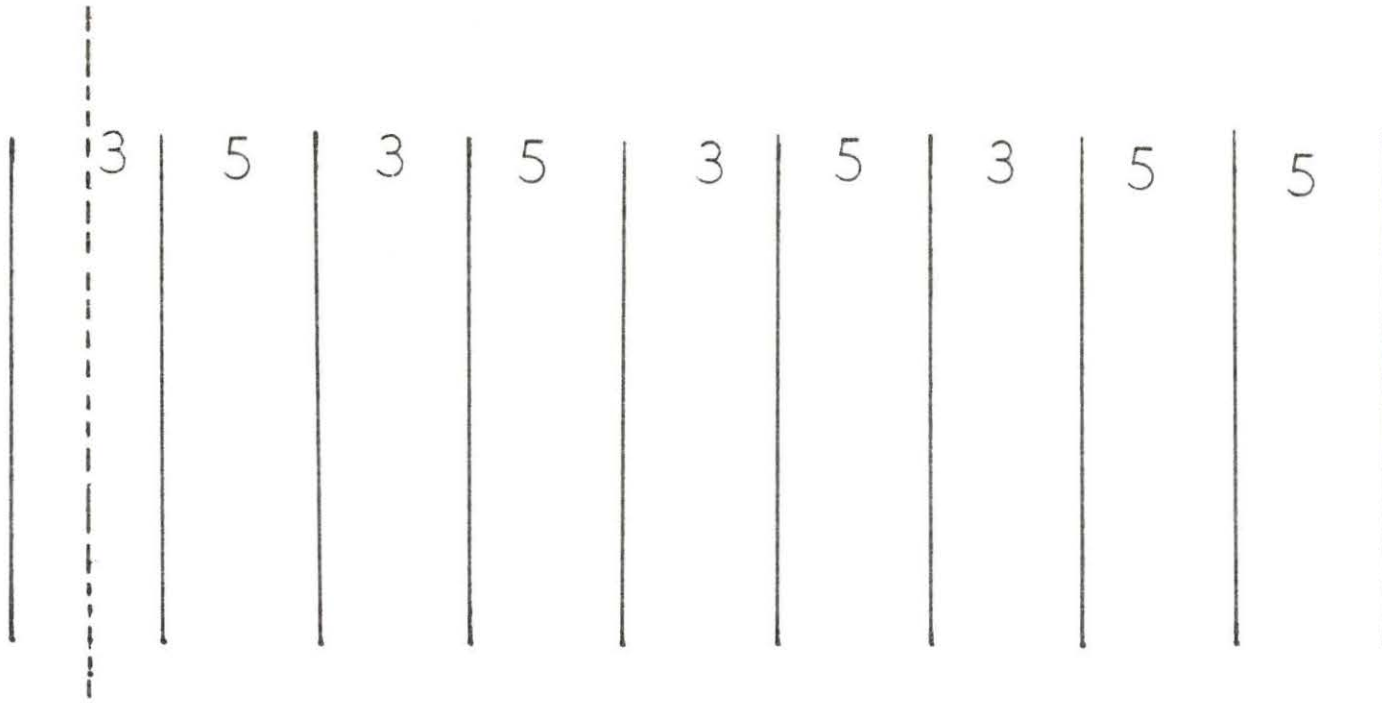
Figure 24.   Node configuration with burnable poison only in assembly of type 3

4. <u>Regular</u> <u>configuration</u> <u>with</u> <u>eight</u> <u>nodes</u>

The outer fuel assembly of type 2 was removed from the regular configuration.

5. <u>Regular</u> <u>configuration</u> <u>with</u> <u>eleven</u> <u>nodes</u>

The two outer fuel assemblies of types 2 and 1, respectively, were divided into two nodes each. Fig. 25 shows the node disposition.

This problem was undertaken in order to study the extension of the model to a larger core.

The results of all the above problems are illustrated in Figs. 26-35. From the flux profiles, we note some deviation between the model and the fine mesh results. An attempt to solve these discrepancies would be to go to higher accuracy such as 10E-7. The corresponding results are displayed in Figs. 36-43. They show a perfect agreement between the two models.
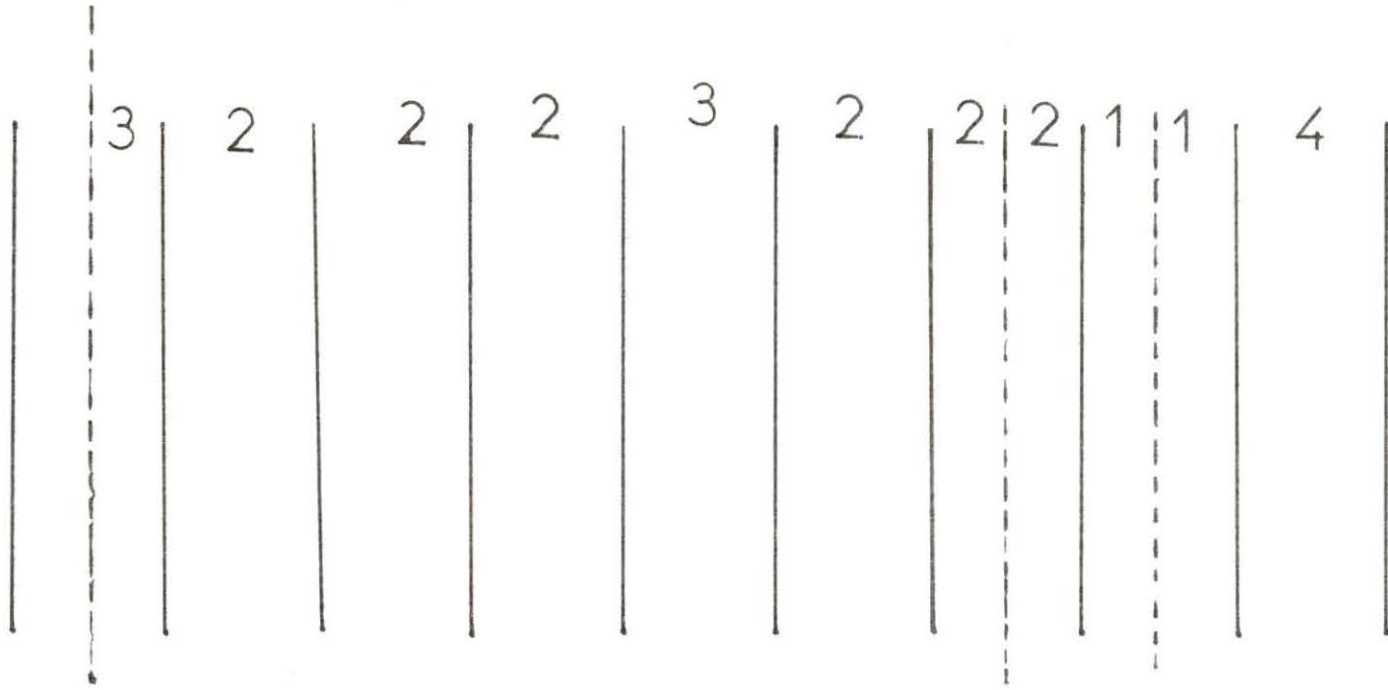
Figure 25. Half core arrangement with eleven nodes
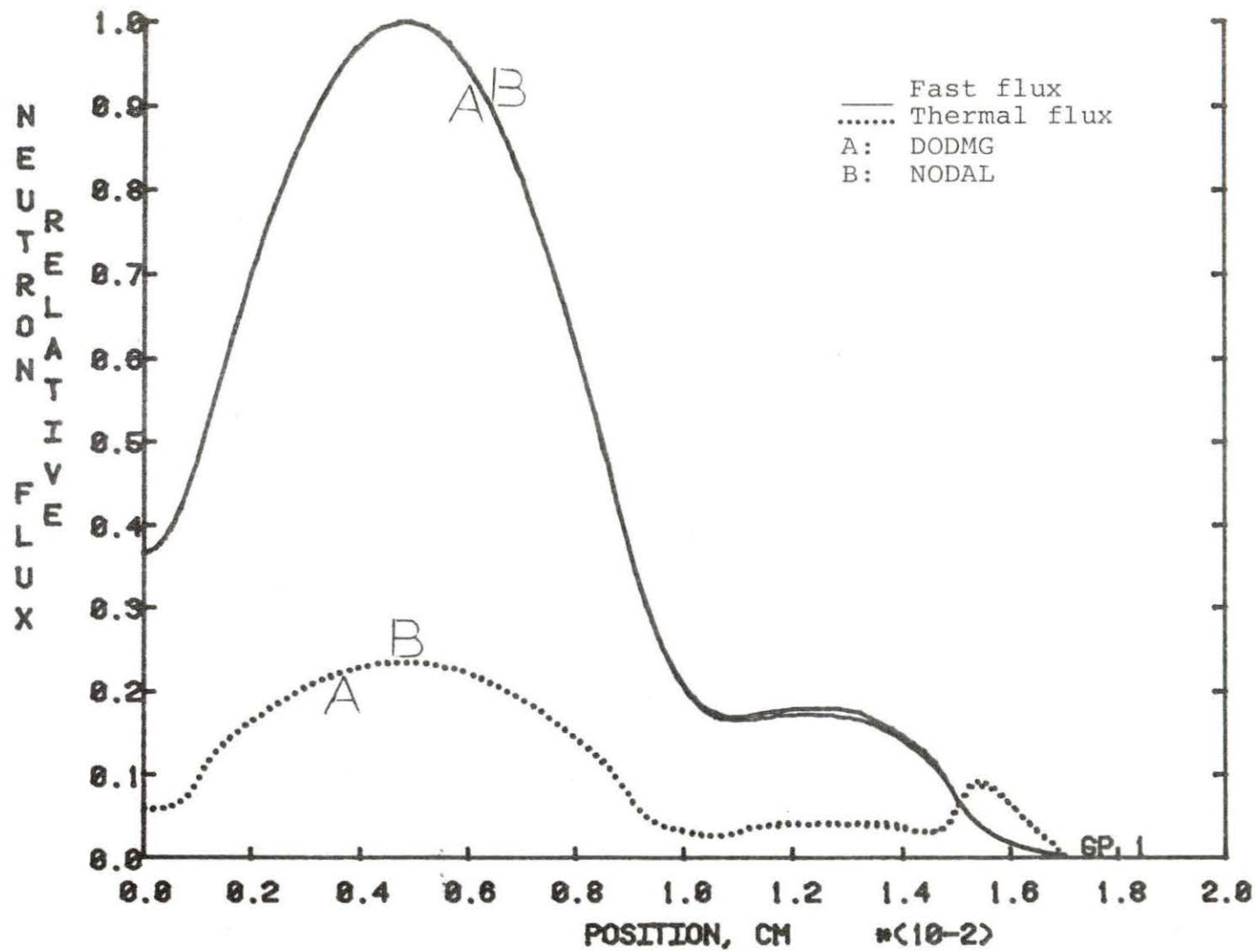
Figure 26. Flux profiles for the configuration where two assemblies are shuffled
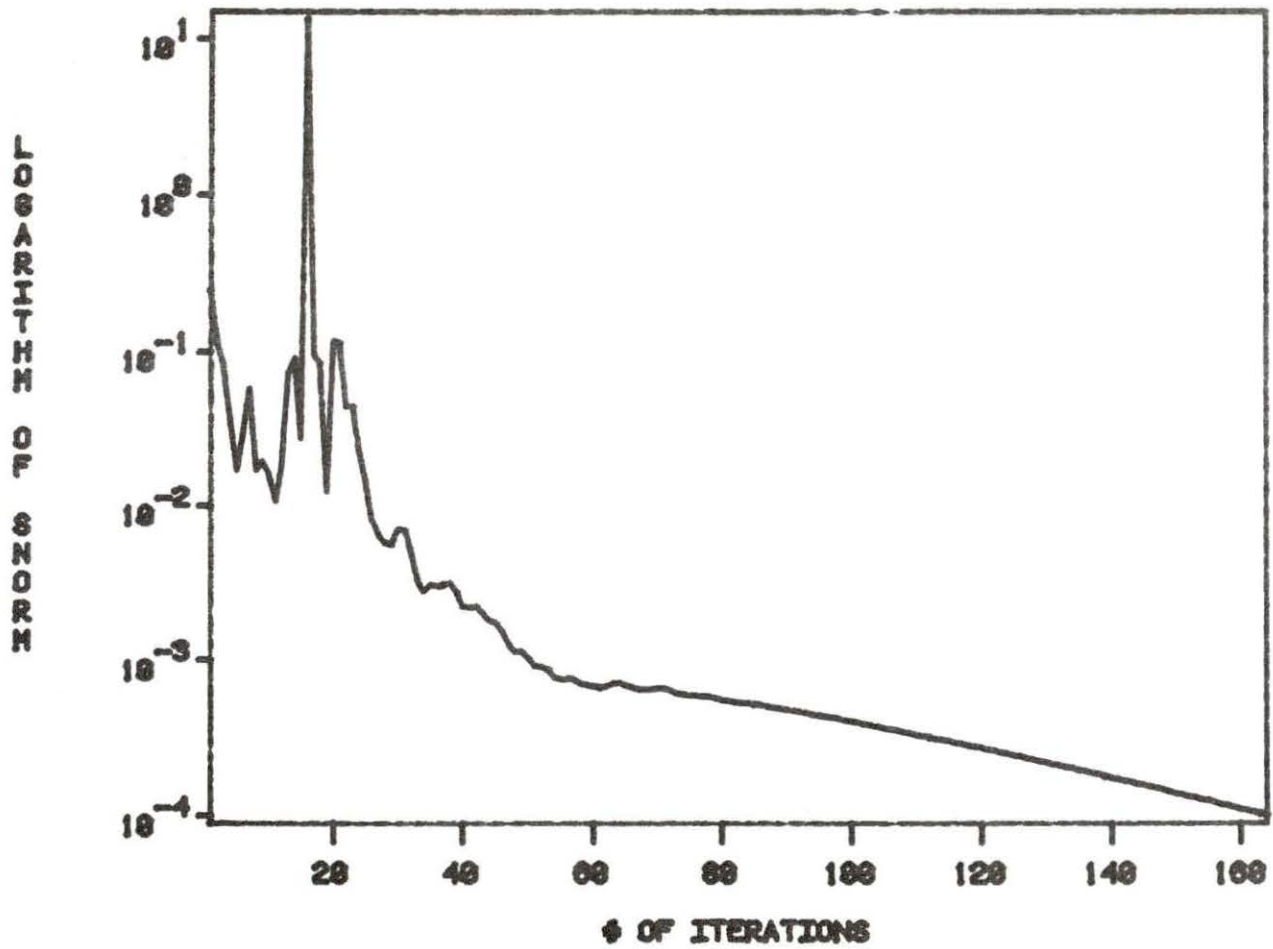
Figure 27. SNORM for the configuration where two assemblies are shuffled
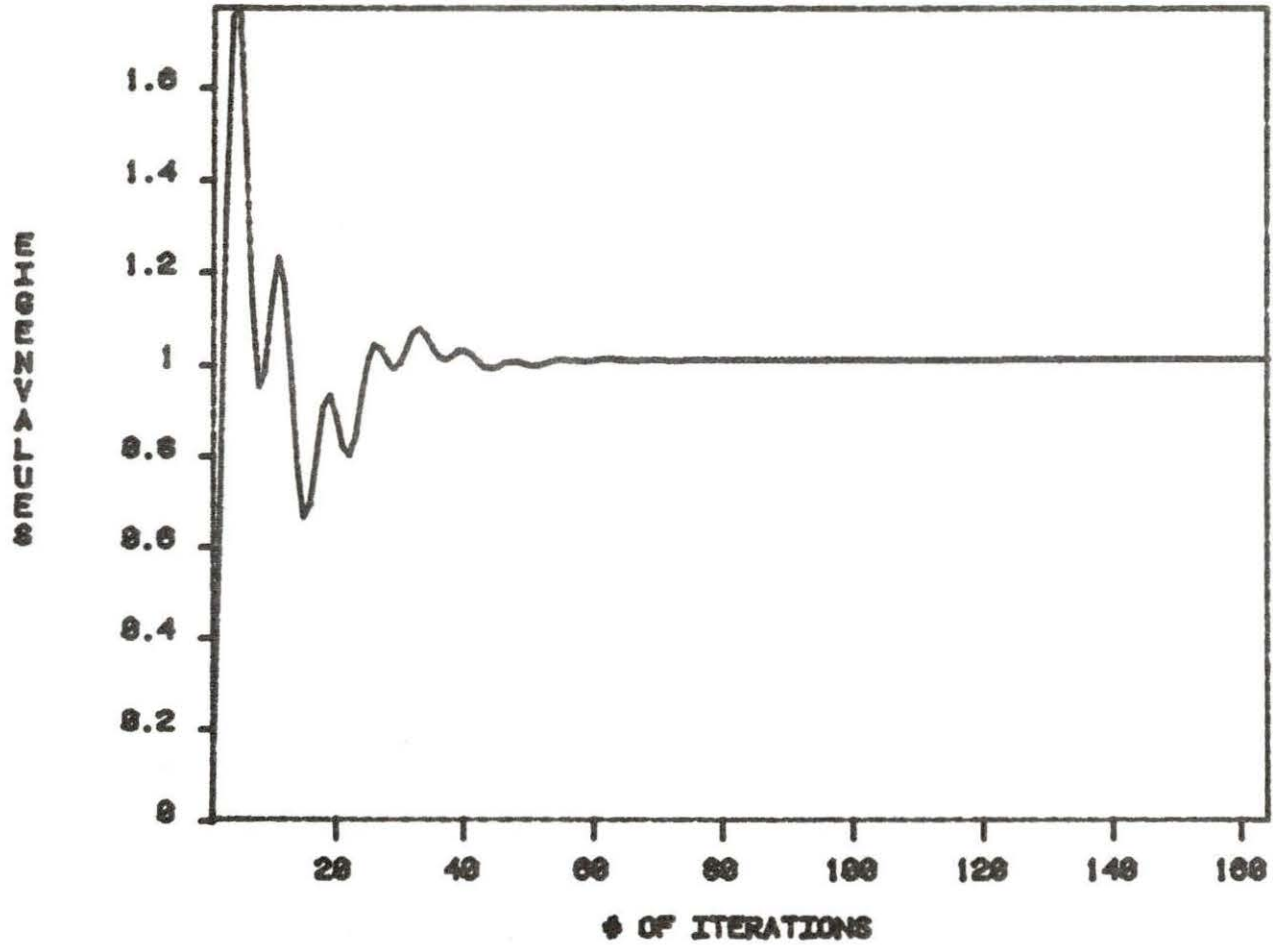
Figure 28. Eigenvalue convergence for the configuration where two nodes are shuffled
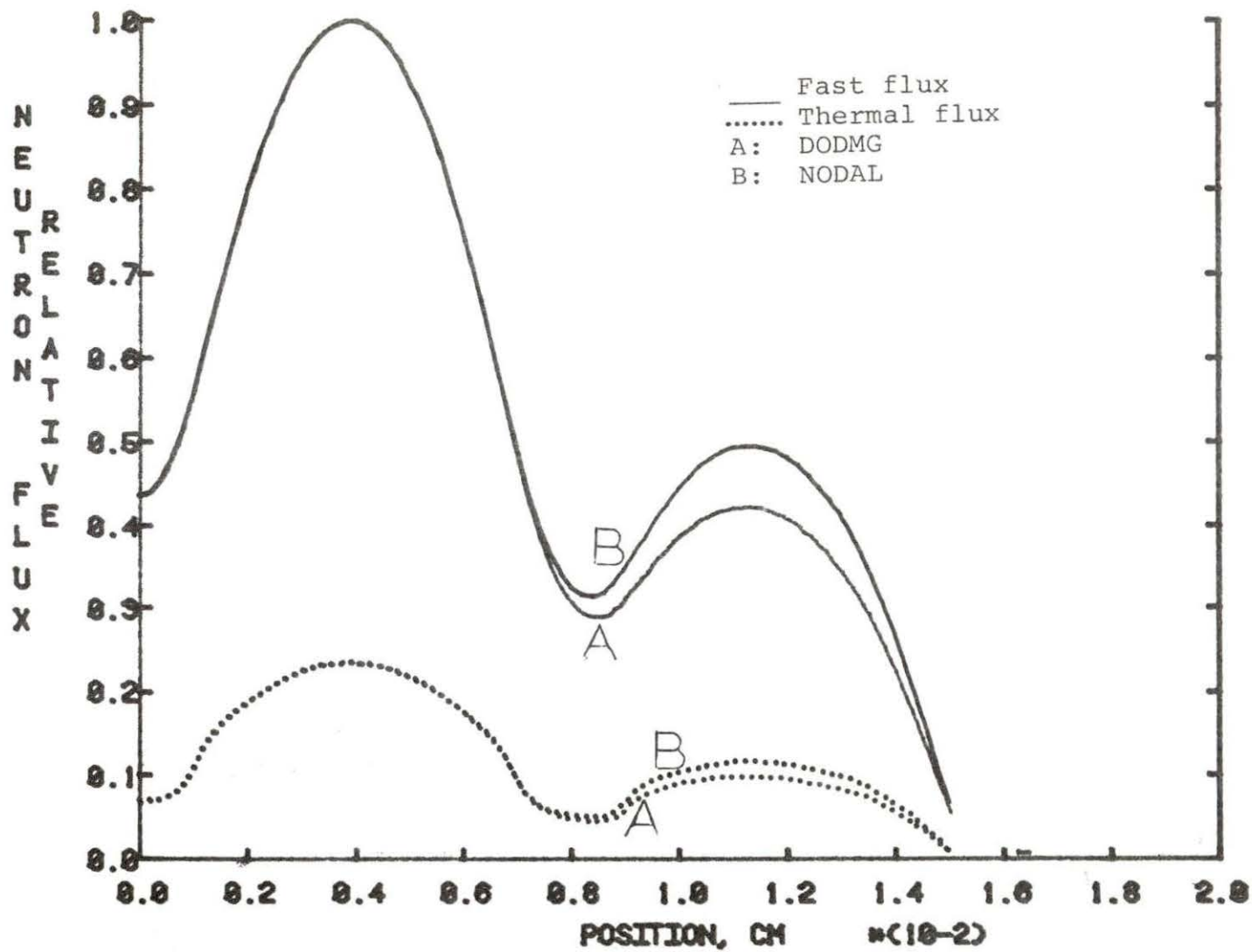
Figure 29. Flux profiles for the regular configuration without reflector
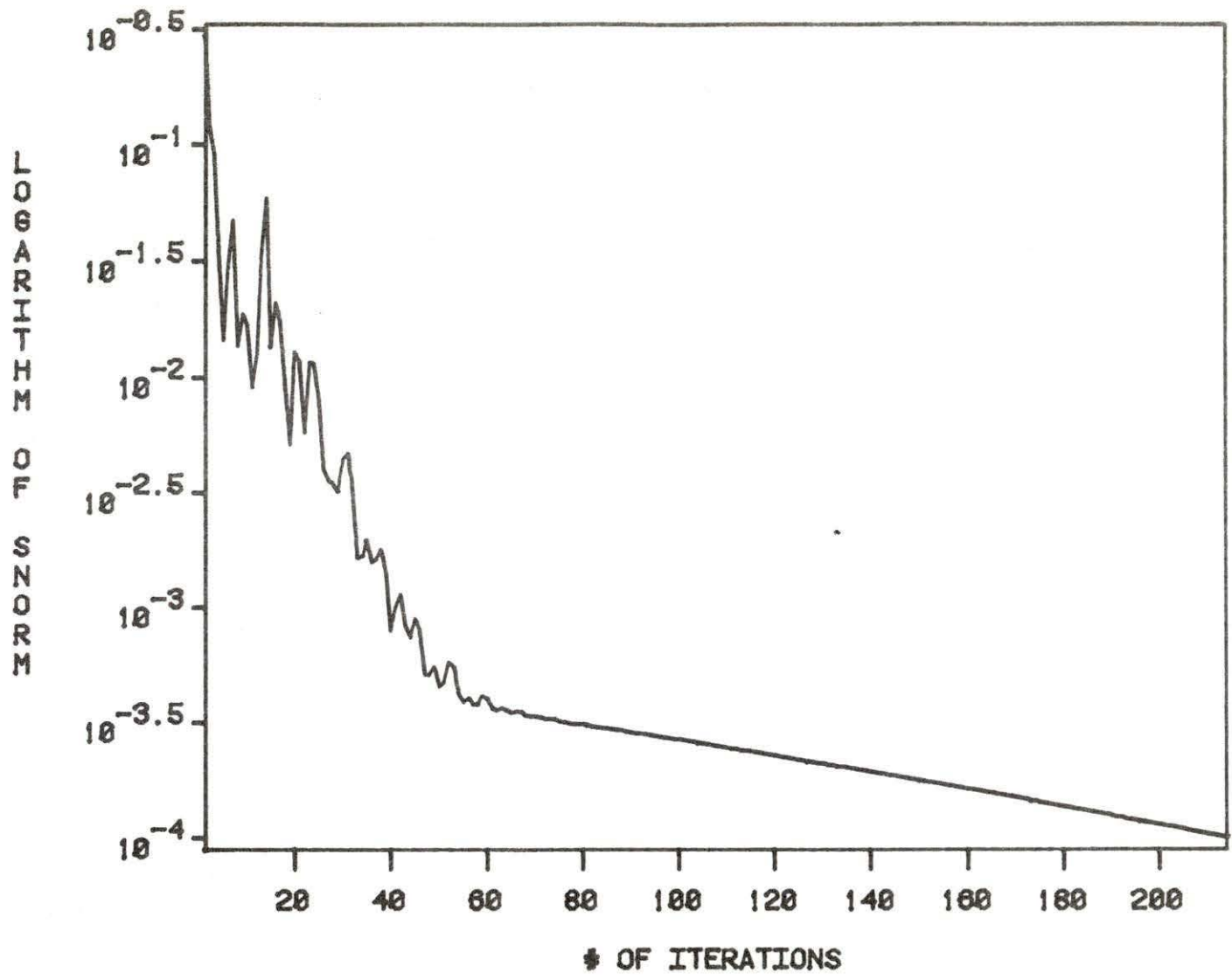
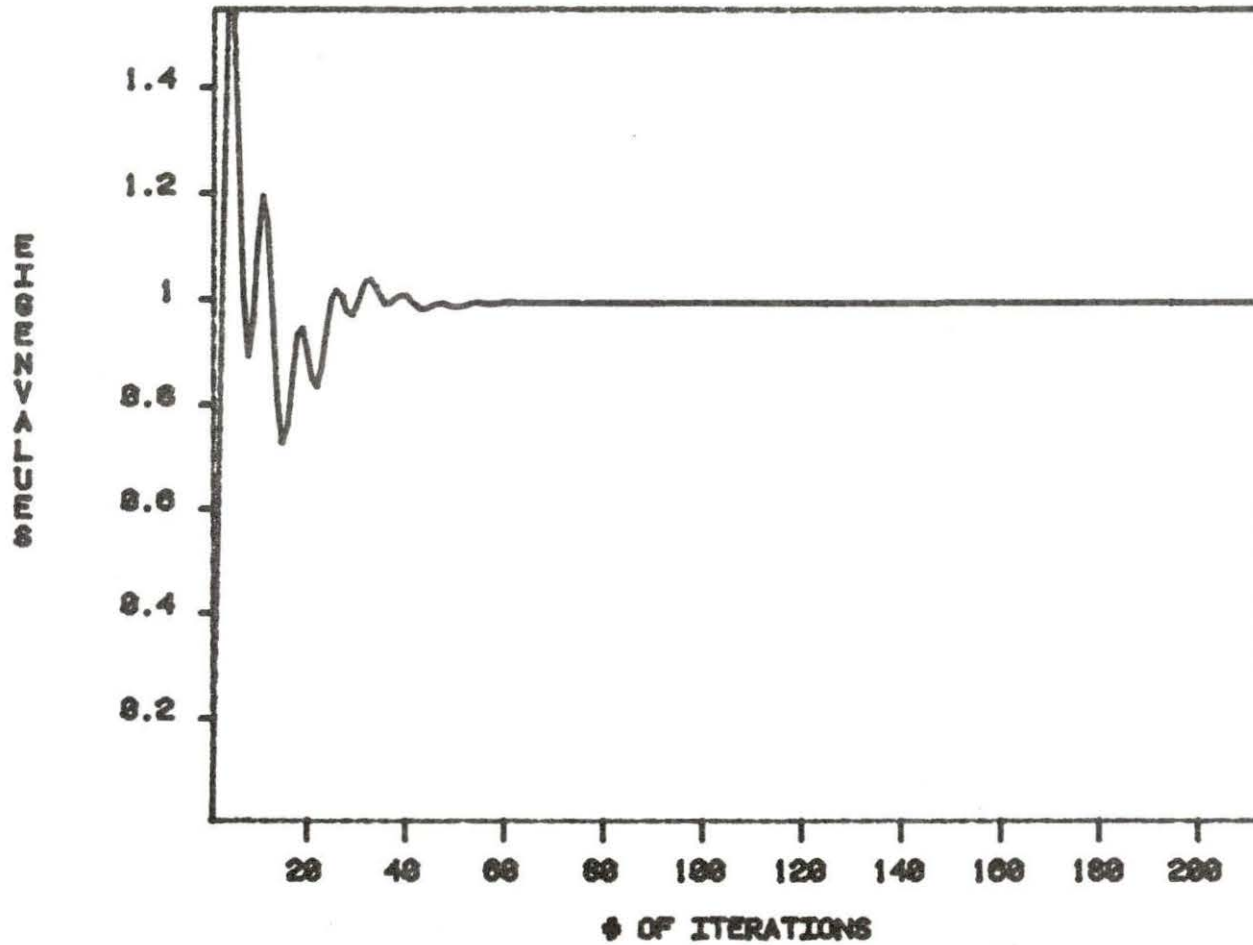Figure 30. SNORM of the regular configuration without reflector

Figure 31.   Eigenvalue convergence for the regular configuration without reflector
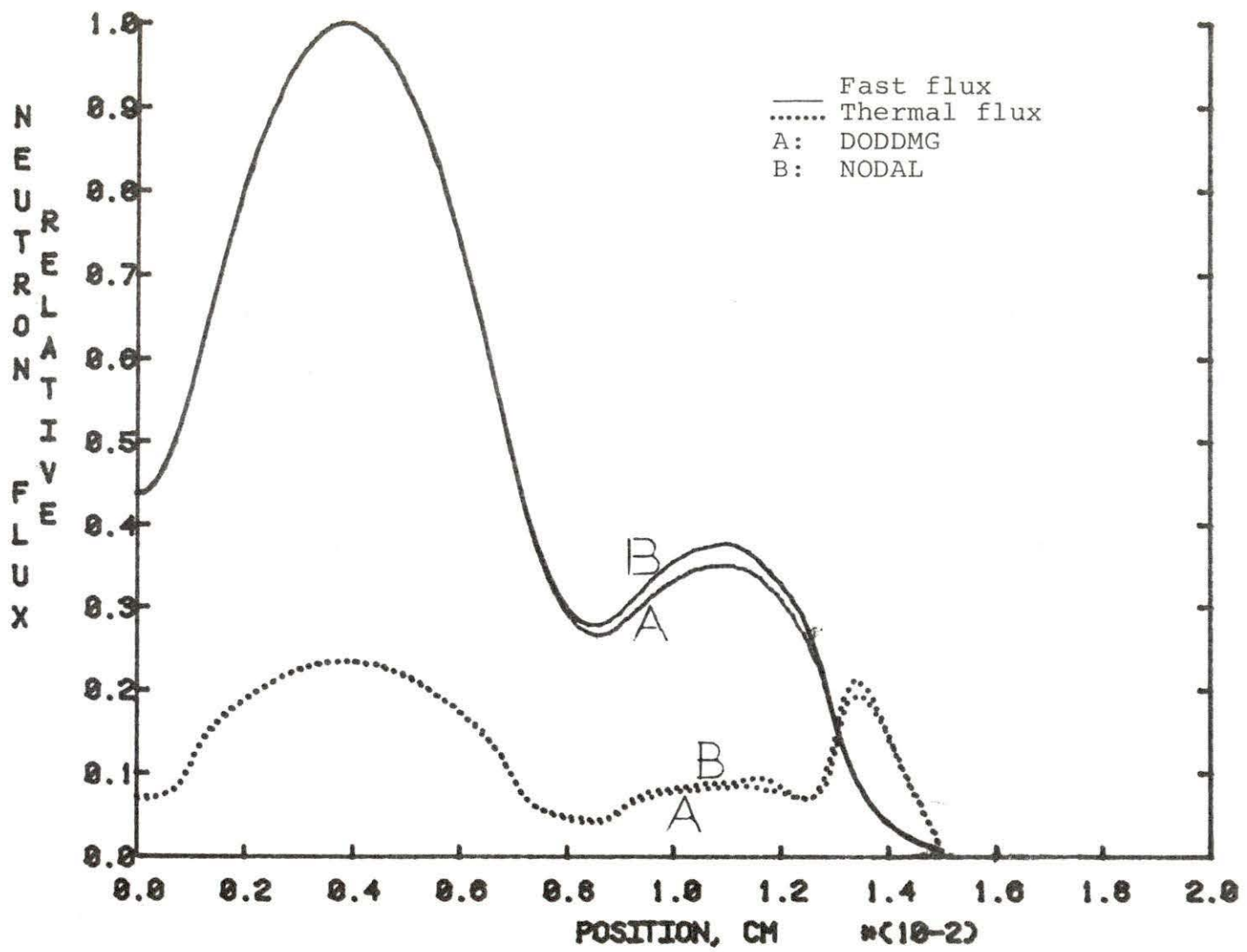
Figure 32. Flux profiles for regular configuration with eight nodes
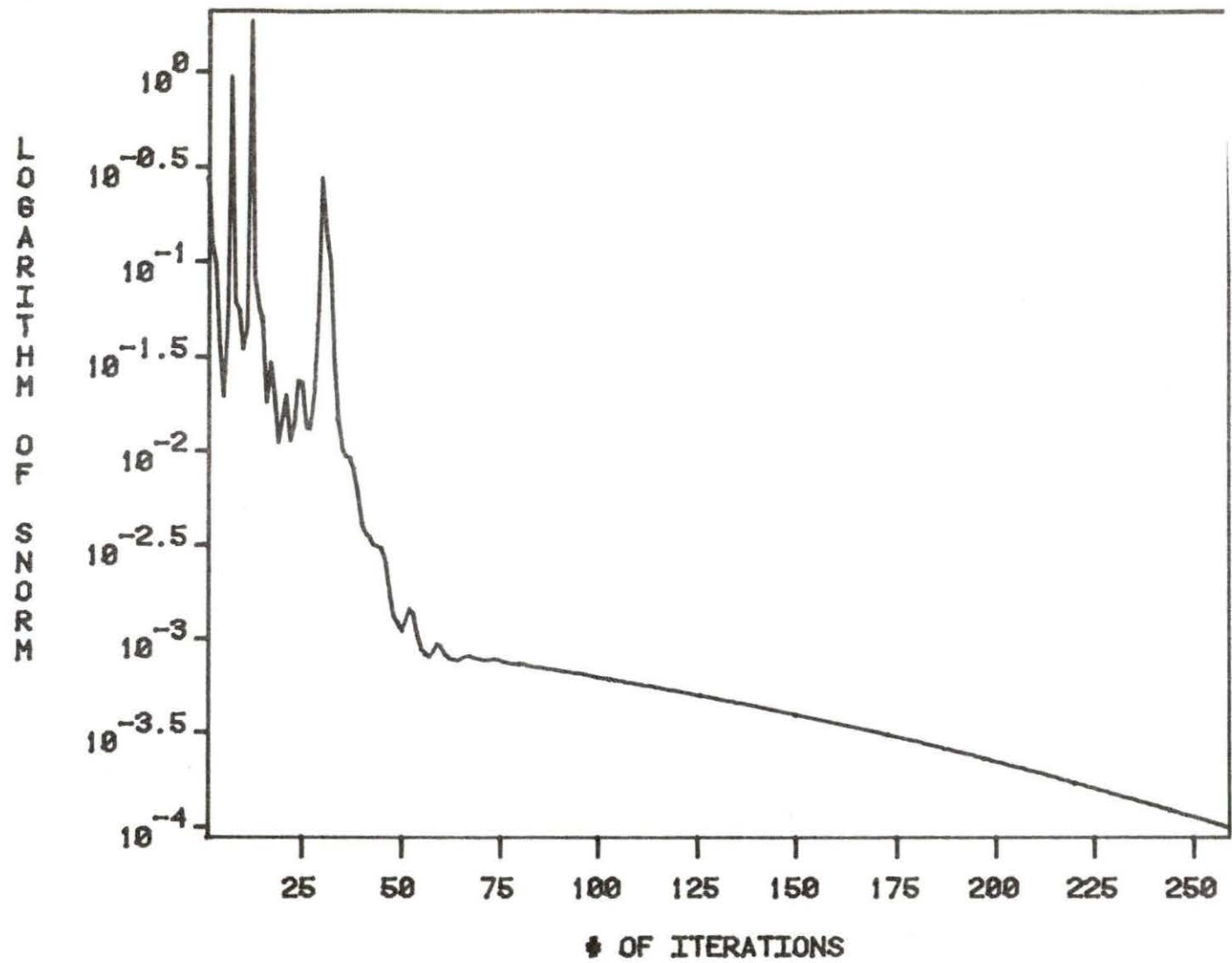
Figure 33. SNORM for regular configuration with eight nodes
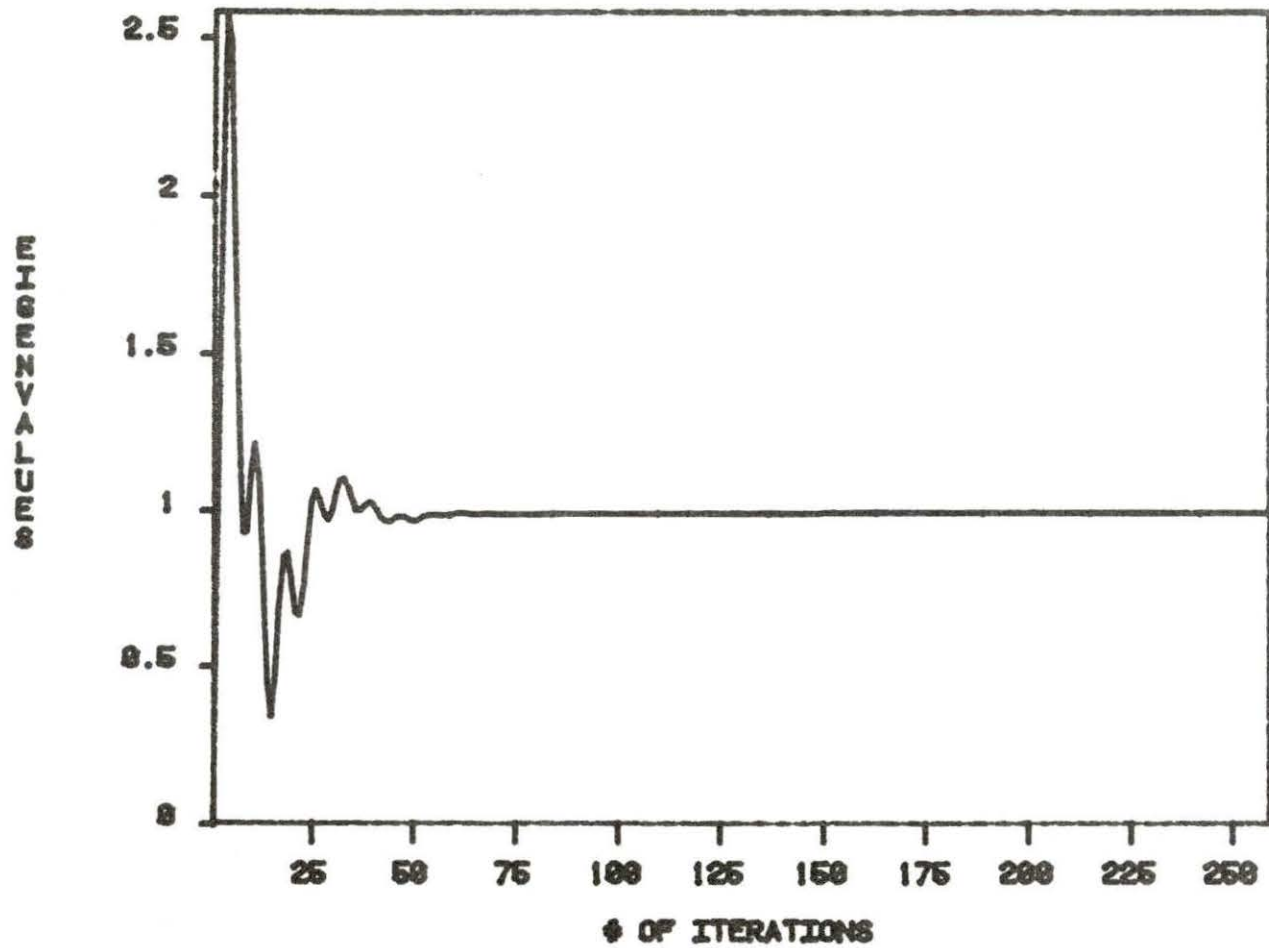
Figure 34.   Eigenvalue convergence for regular configuration with eight nodes
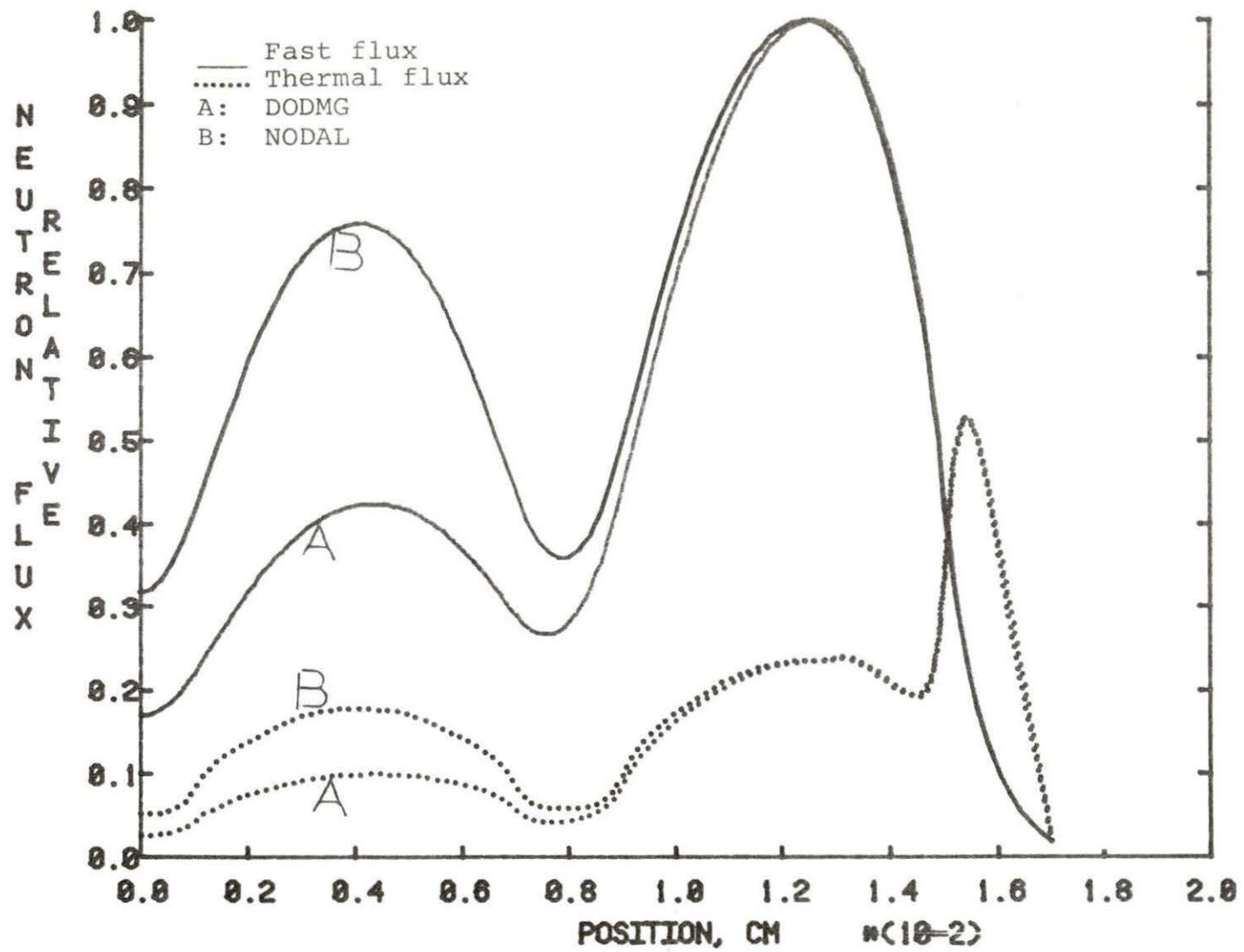
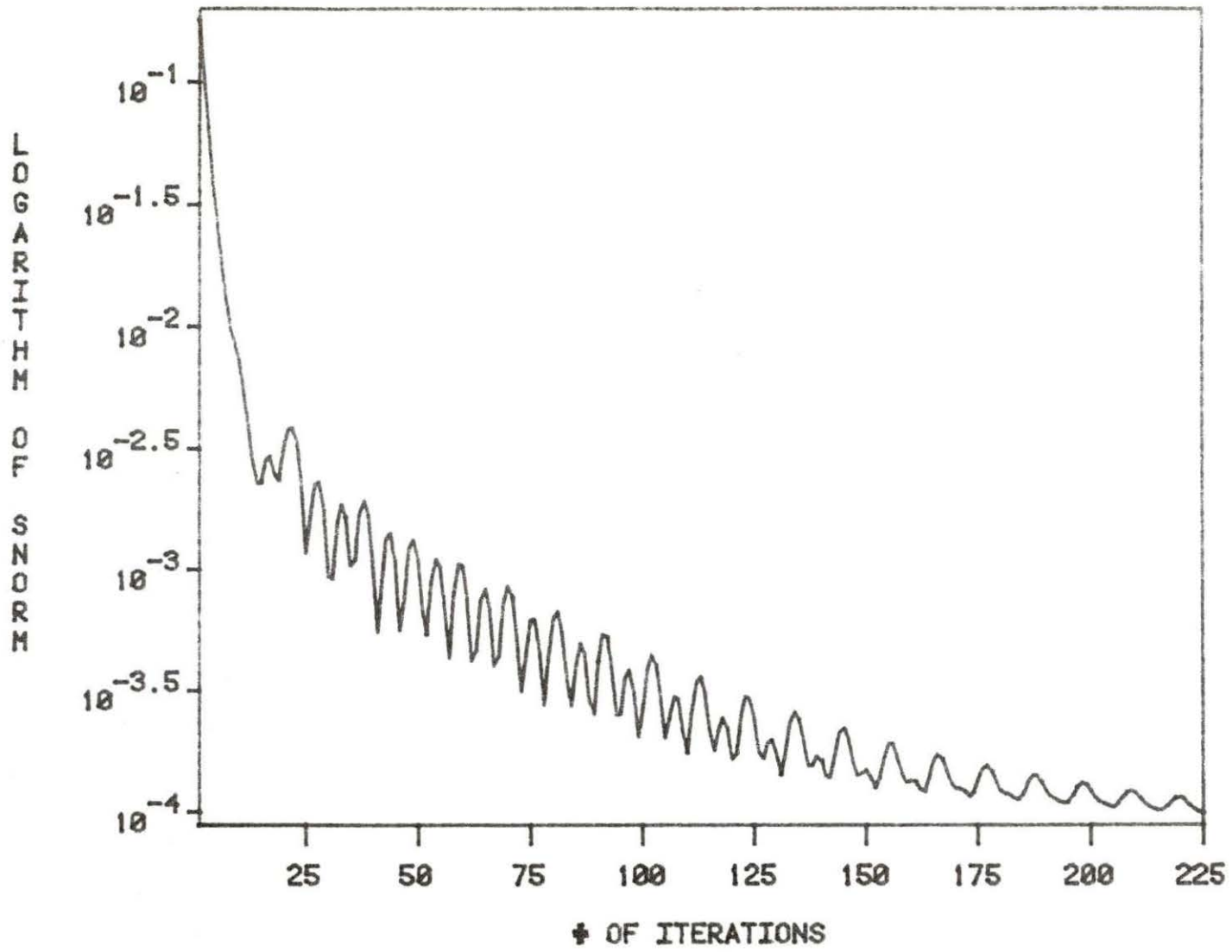Figure 35. Flux profiles for configuration with eleven nodes

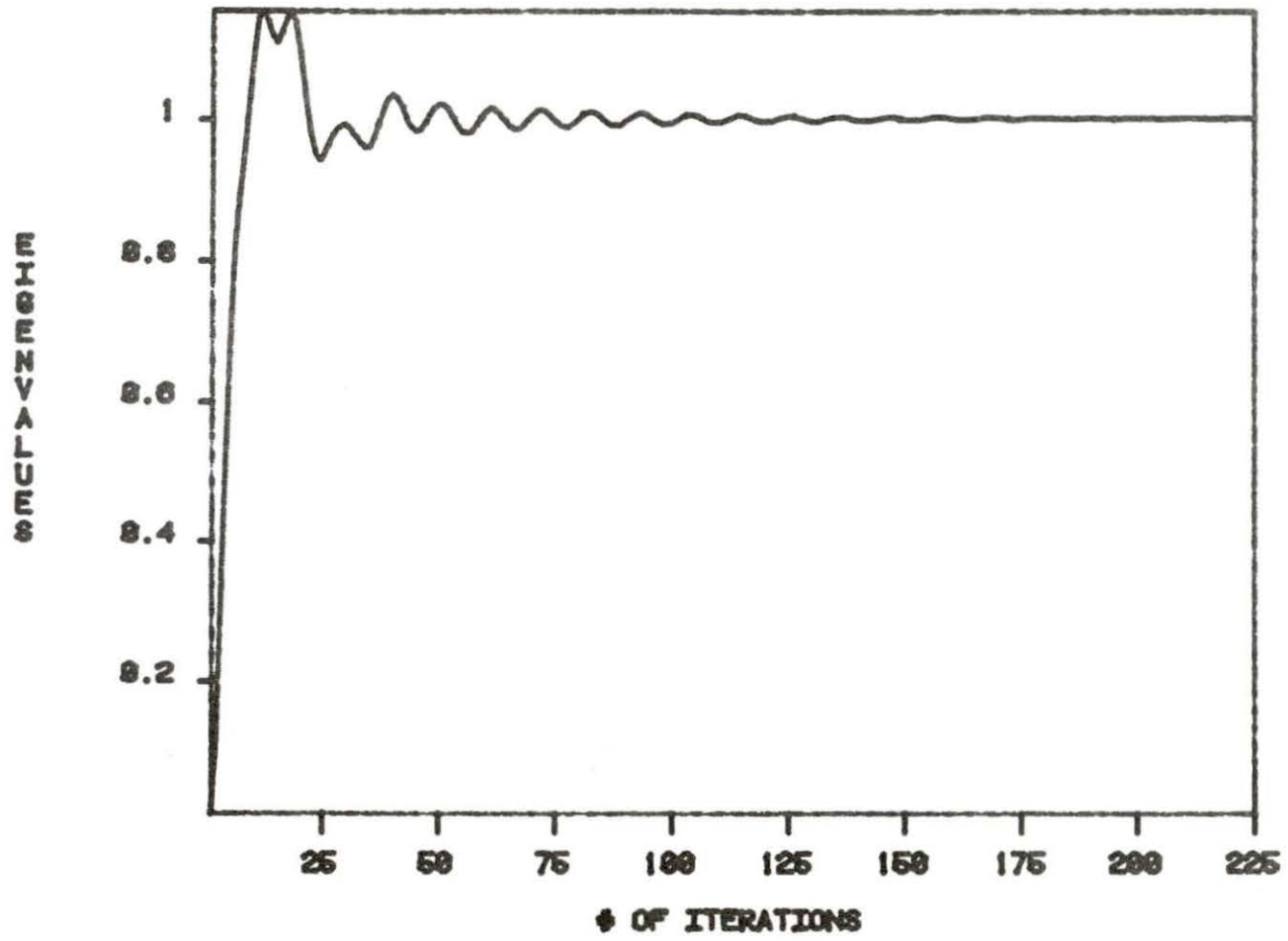Figure 36.   SNORM of the configuration with eleven nodes

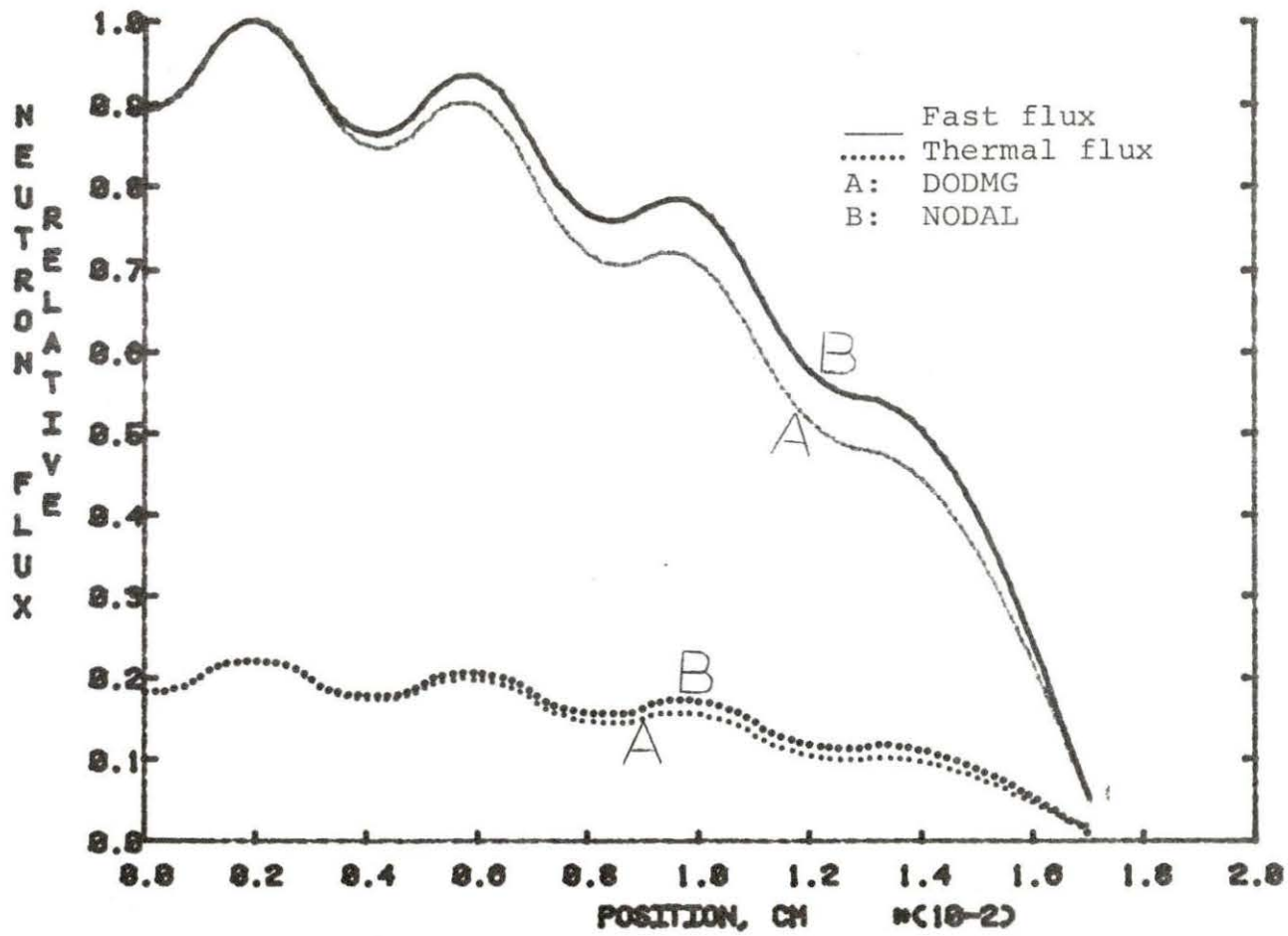Figure 37. Eigenvalue convergence for the regular configuration with eleven nodes

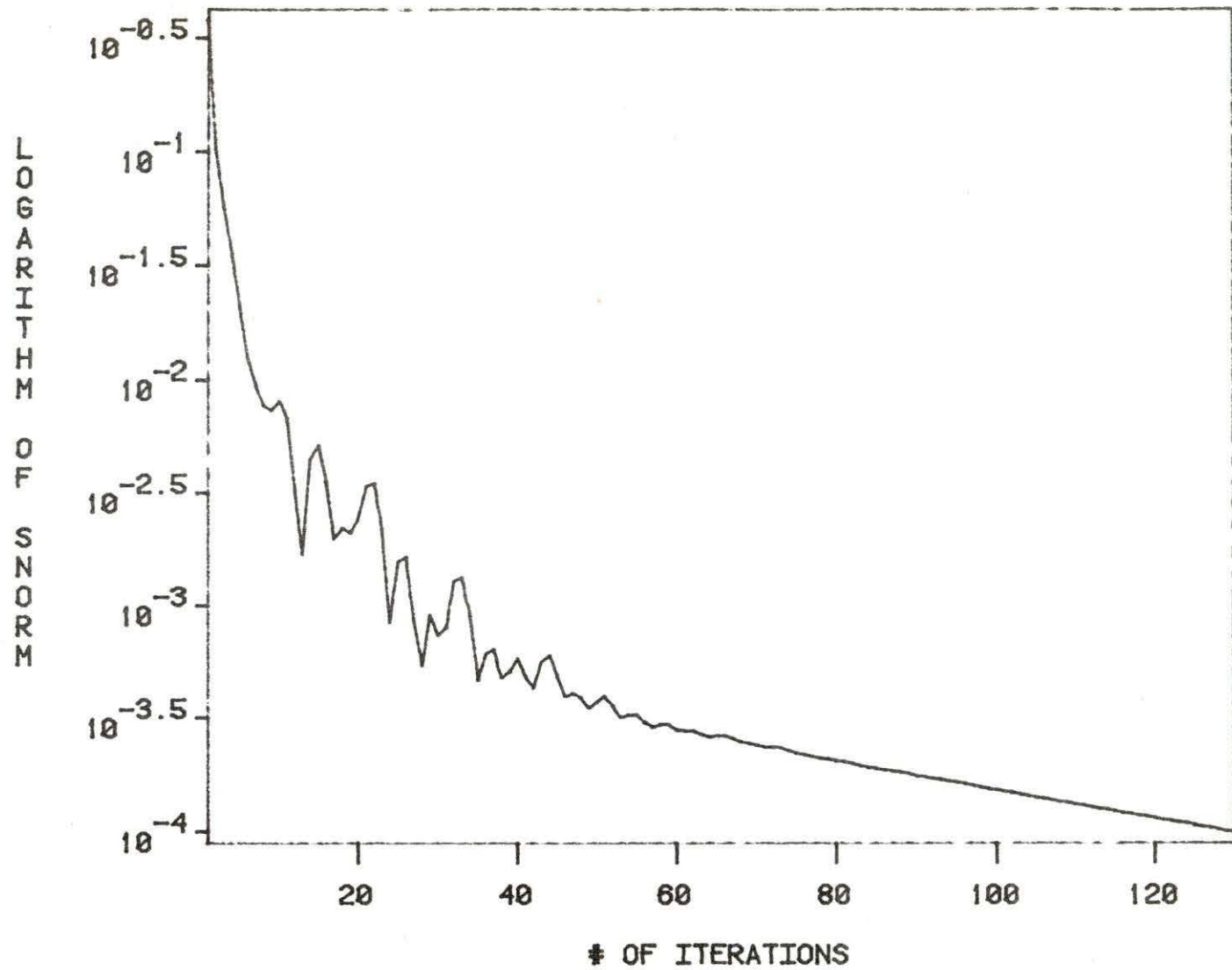Figure 38. Flux shapes for configuration with burnable poison

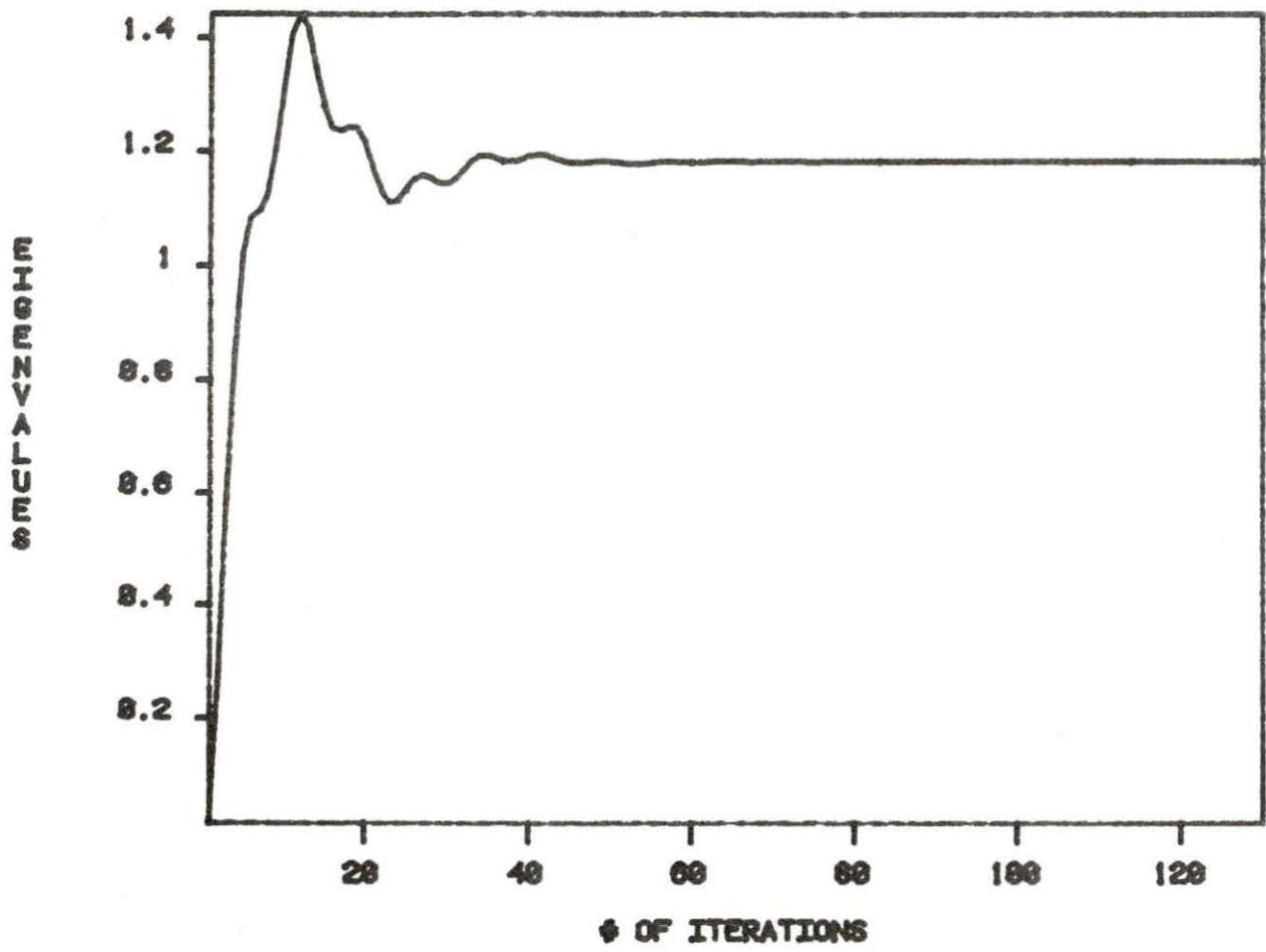Figure 39. SNORM for configuration with burnable poison

Figure 40. Eigenvalue convergence for configuration with burnable poison
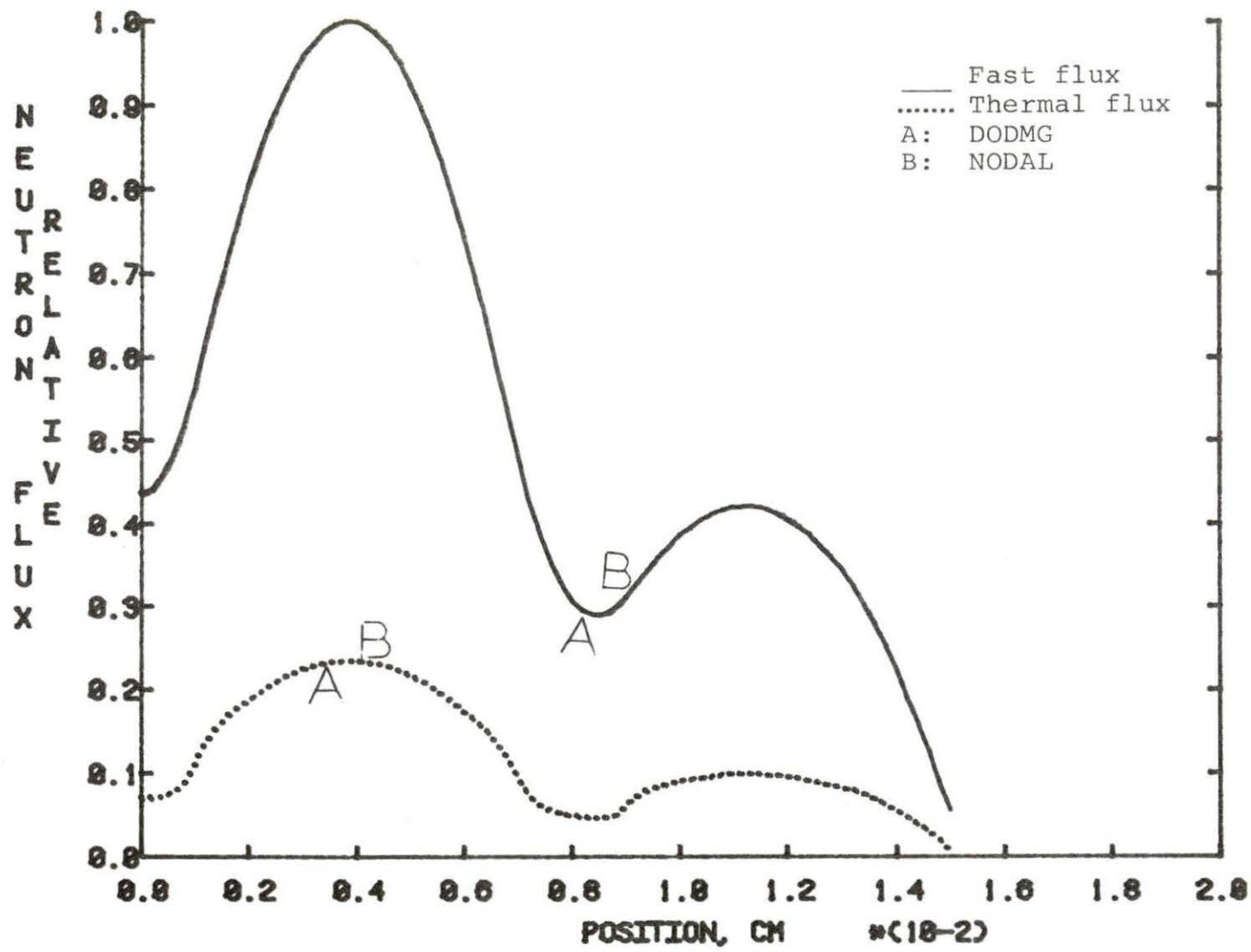
Figure 41. Flux profiles of regular configuration without reflector
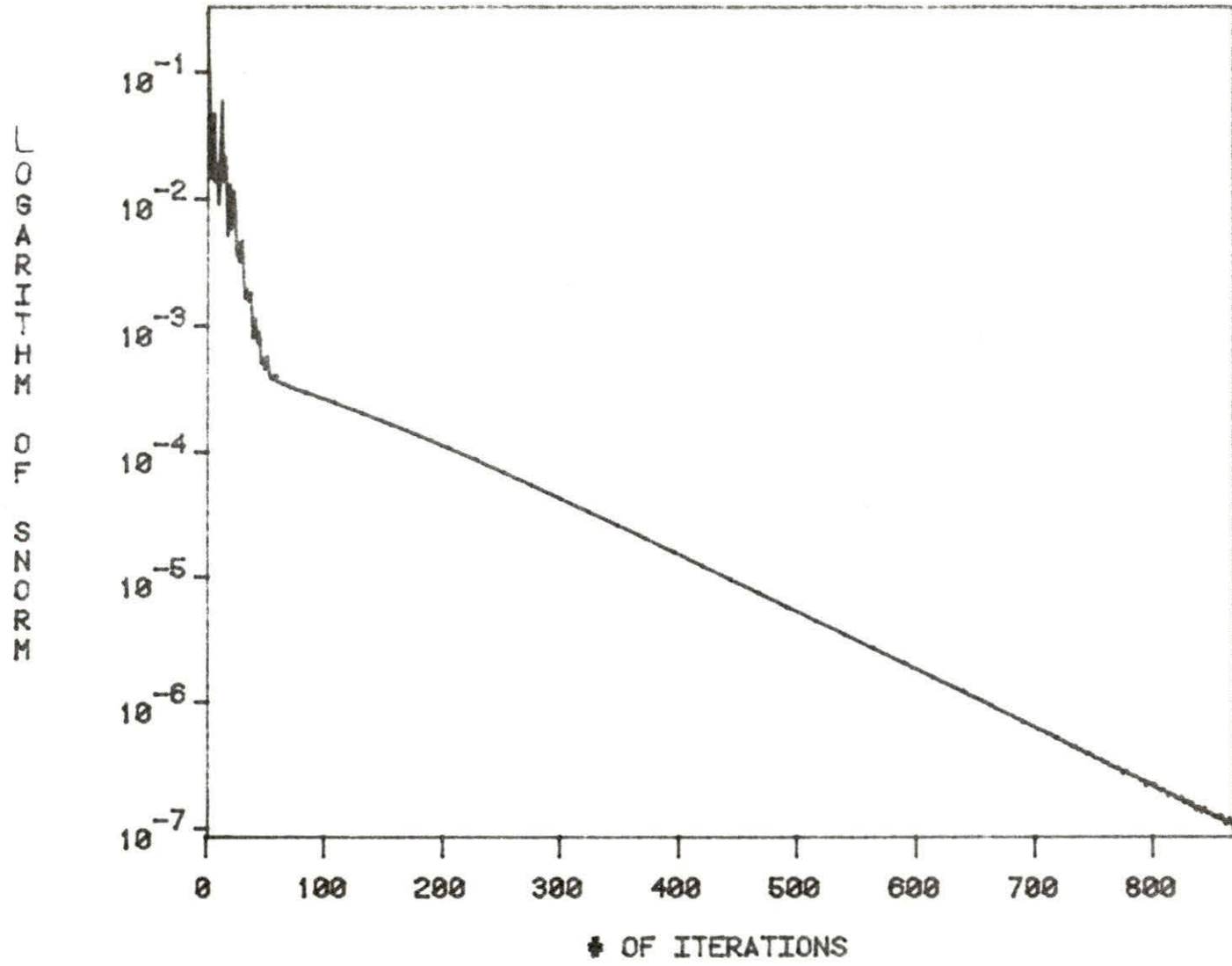
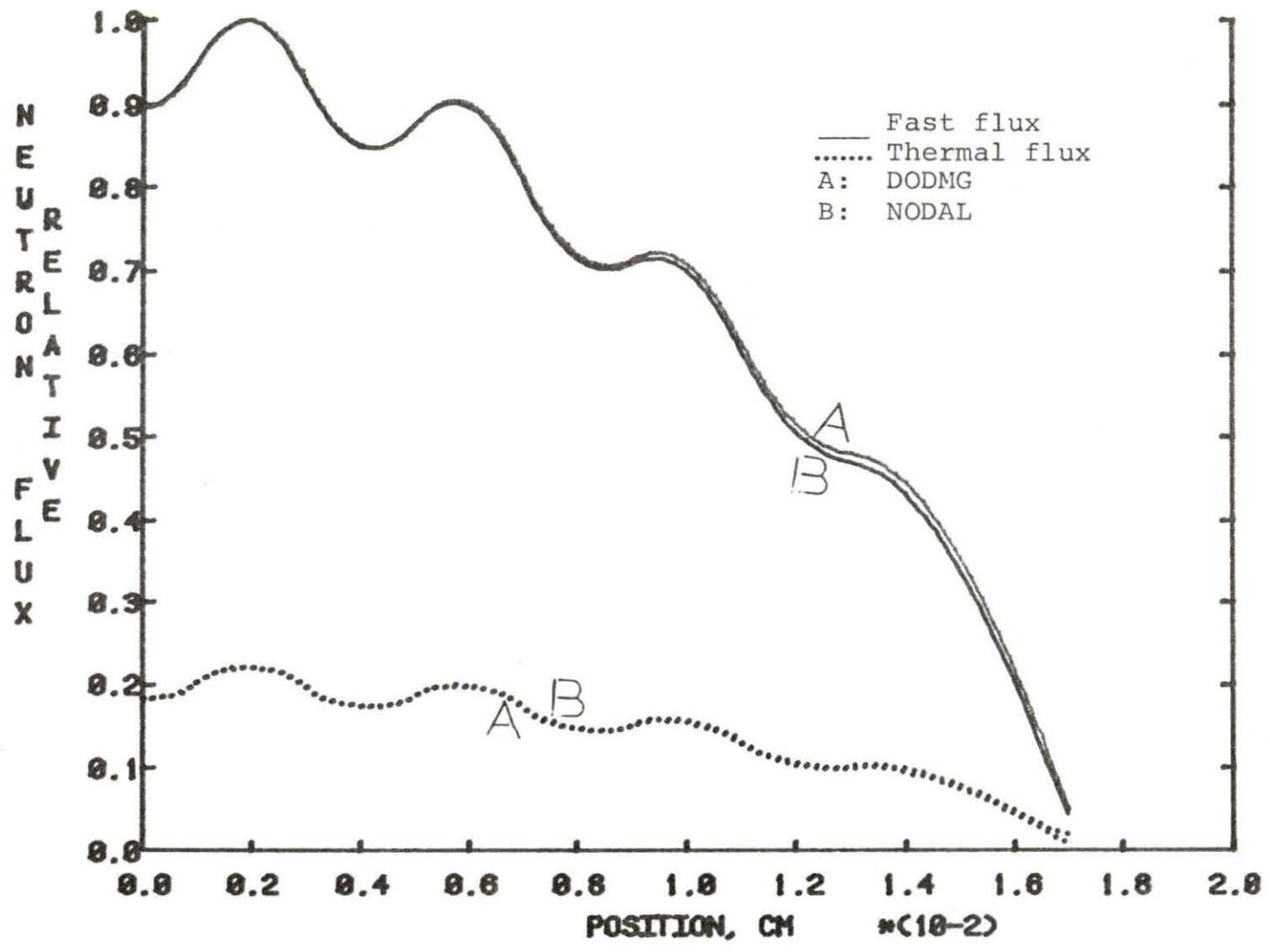Figure 42.   SNORM of configuration without reflector

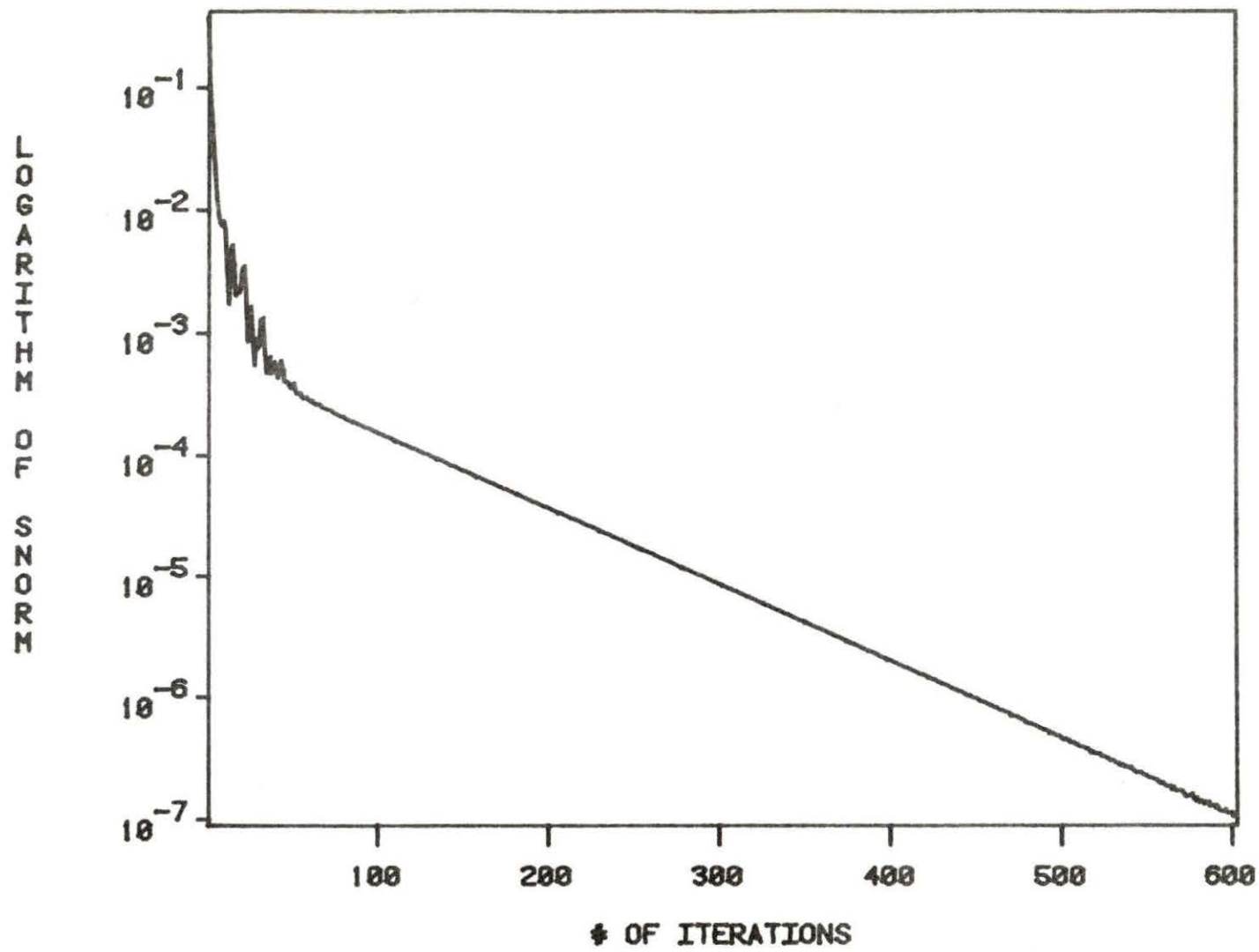Figure 43. Flux profile comparison for configuration with burnable poison

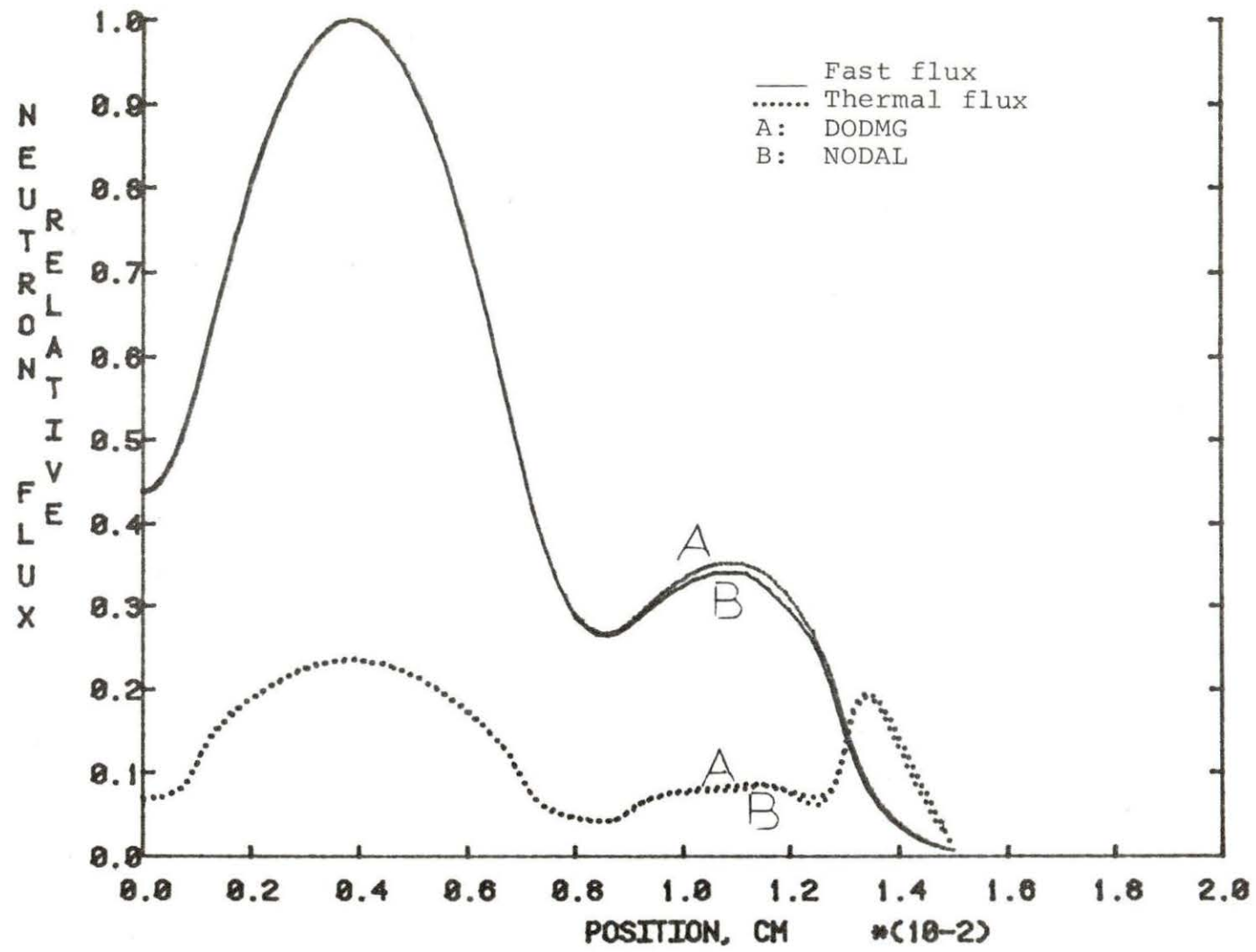Figure 44. SNORM of configuration with burnable poison

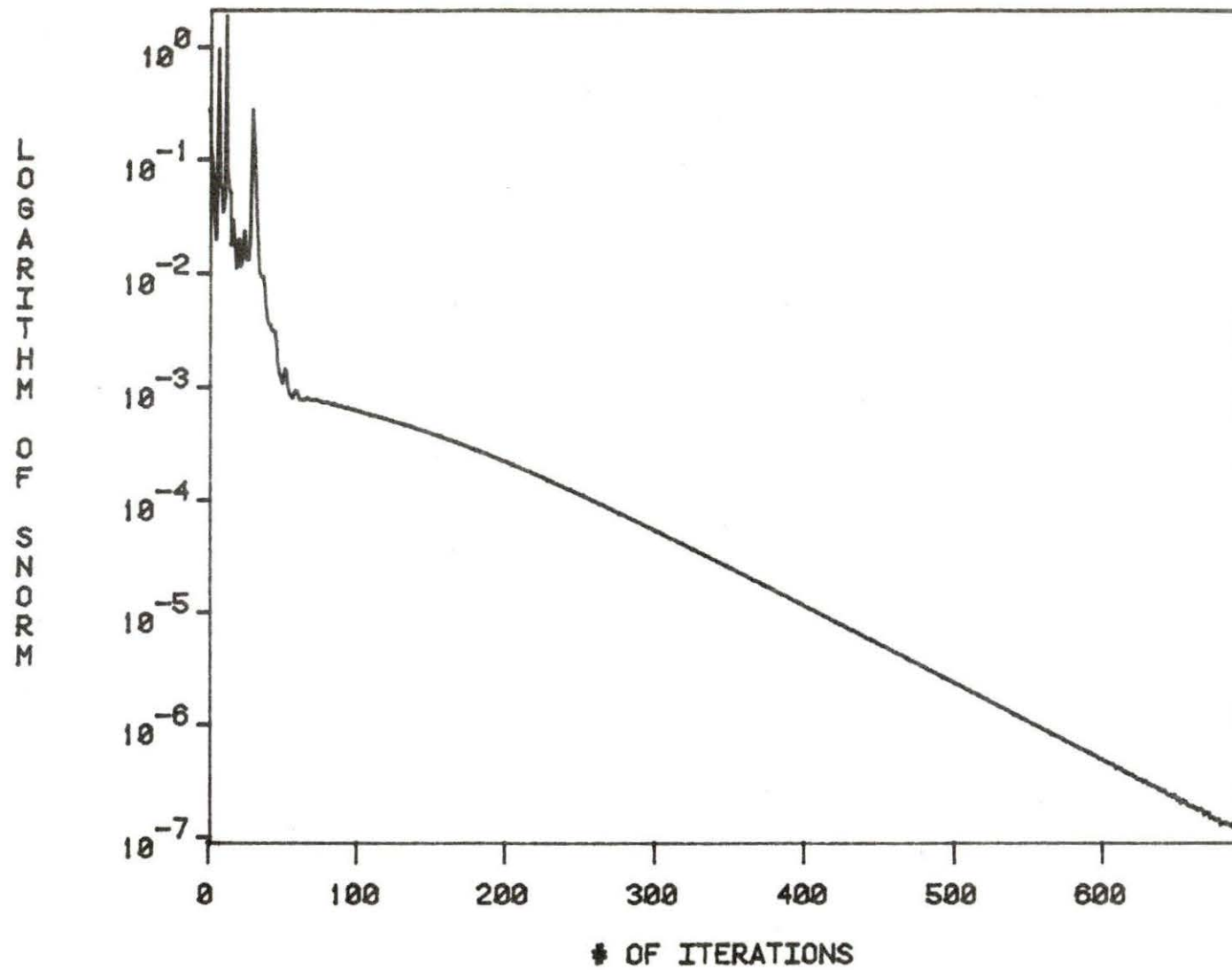Figure 45. Flux profiles for configuration with eight nodes

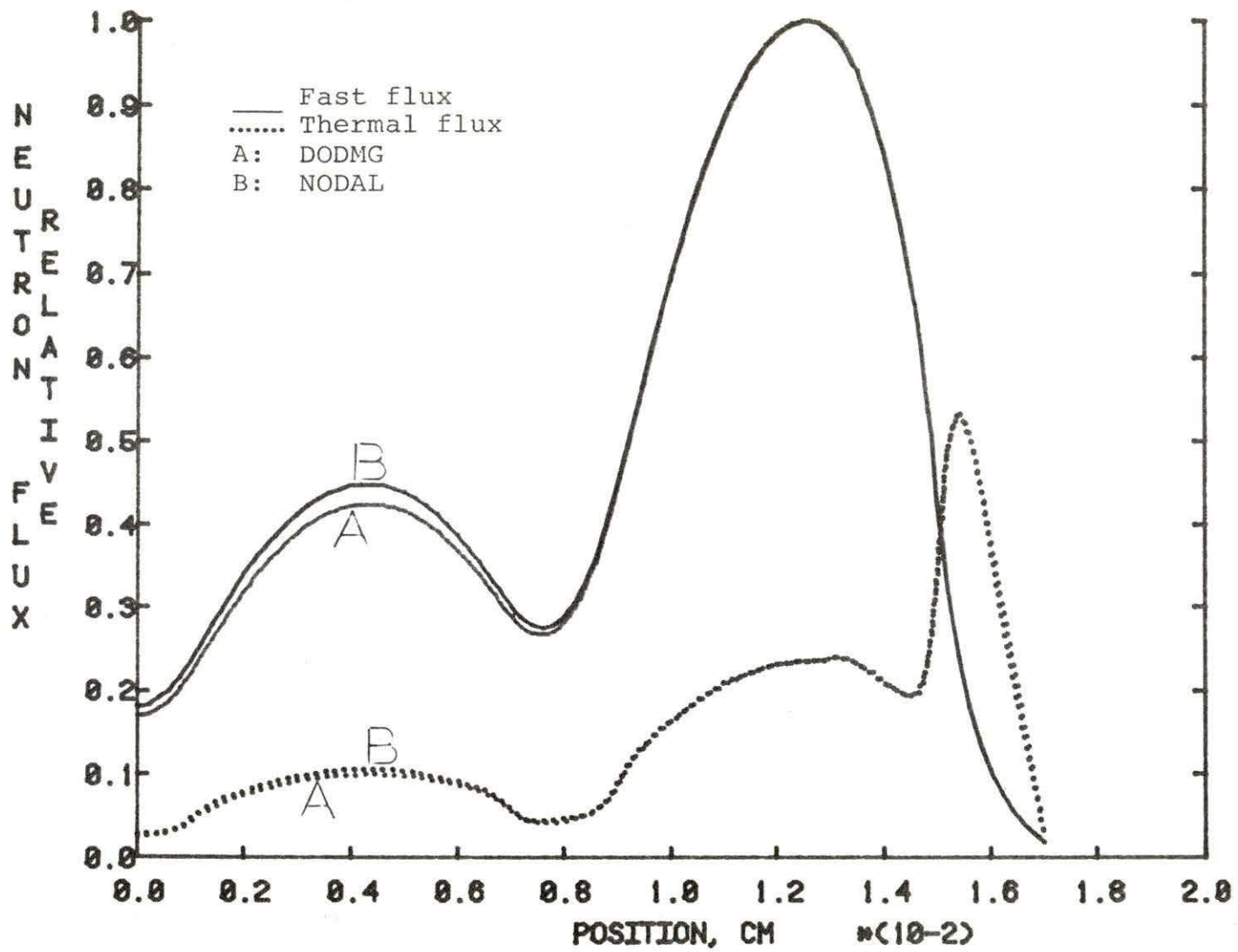Figure 46.   SNORM of configuration with eight nodes

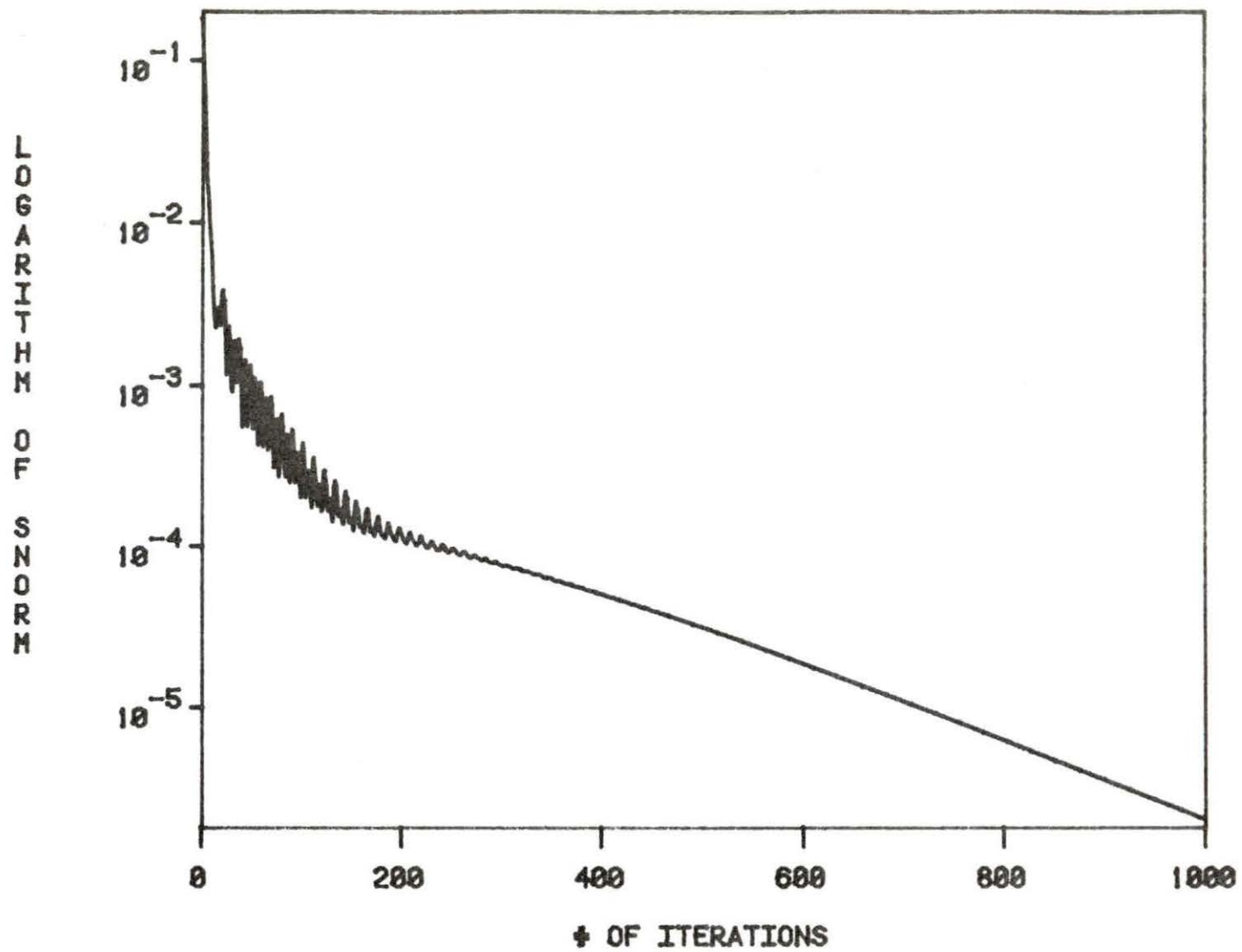Figure 47. Flux profiles for configuration with eleven nodes

Figure 46. SNORM of configuration with eleven nodes

V. SUMMARY AND CONCLUSIONS

The second order fitting has shown some shortcomings in all cases except for the problem where the reflector was removed and a vacuum boundary condition applied. The convergence criterion was 10E-6; therefore, we didn't try a lower one.

The amelioration of the model was gained by the use of the fourth order expansion. Nevertheless, the number of iterations needed for convergence was relatively high (200 iterations) for a moderate convergence criterion (10E-4). The attempt of decreasing it to 10E-7 didn't resolve the difficulty, and the problem took more than a thousand iterations to converge.

The experimental method was considered and applied to each parameter separately. The optimization procedure time was relatively small when previous results were used. Its application reduced the number of iterations needed for the problem to converge to only 65 iterations with a tolerance of 10E-4.

We also found that the accelerating technique selected was improved very simply by the use of the SNORM which is easily calculated.

The study of various problems was performed and insured the feasibility of the optimization technique results. The use of the optimal factors gave excellent results for the

case where two fuel assemblies were shuffled, even though the convergence criterion was 10E-4.

For the remaining problems, the convergence was attained for about 200 iterations and the conformity with respect to DODMG may be acceptable. Therefore, one needed to augment the accuracy to 10E-7, so the matching between the two models was excellent. Unfortunately, the computation time increased, especially for the problems where the number of nodes varied (8 nodes and 11 nodes cases). This suggests that the model will be most efficient in fuel management where the assembly shuffling is frequent. Also, the use of a moderate convergence criterion such as 10E-4 was enough for some problems (regular configuration, no reflector configuration).

Another general aspect of the technique is that the SNORM was continuously decreasing. This is a characteristic of the convergence of the solution. Unfortunately, in some cases, this rate of change doesn't remain as large as in the beginning of the process.

VI.   SUGGESTIONS FOR FURTHER STUDIES

Four major studies may be done to ameliorate this
model.   These are:

(1)   Attempt to damp the oscillations accused by the
      SNORM and eigenvalue curves.   One has to investi-
      gate the effect of the interface condition on
      this problem.

(2)   Further study is needed to incorporate into the
      program the experimental technique that has been
      applied.

(3)   Apply the model to problems where the diffusion
      coefficient is variable and the cross sections
      are burnable dependent.

(4)   Finally, a more interesting case to investigate
      is the extension of the method to the three-
      dimensional case and the n groups energy diffu-
      sion equation, which is a more realistic problem.

VII. BIBLIOGRAPHY

1. J. Askew, "Summary of the meeting" in Calculation of 3-Dimensional Rating Distributions in Operating Reactors (Organization for Economic Co-operation and Development, Paris, 1979), p. 13.

2. R. L. Burden, J. D. Faires, and A. C. Reynolds, Numerical Analysis (Prindle, Weber & Shmidt, Boston, Mass., 1981).

3. Numerical Determination of the Space, Time, Angle, or Energy Distribution of Particles in an Assembly, Argonne Code Center: Benchmark Problem Book. Supplement 2. Argonne National Laboratory. June (1977).

4. James J. Duderstadt and Louis J. Hamilton, Nuclear Reactor Analysis (John Wiley and Sons, Inc., New York, 1976).

5. A. F. Rohach, DODMG: Diffusion theory, one dimensional multigroup diffusion program (1982) (Lecture notes, I.S.U., Nuclear Engineering 654).

6. M. J. Clark and K. F. Hansen, Numerical Methods of Reactor Analysis (Academic Press, Inc., New York, 1964).

7. Sue Yih, "Application of accelerated convergence techniques to the neutron diffusion--nodal model," M.S. thesis, Iowa State University, 1981 (unpublished).

8. W. F. Ames, Numerical Methods for Partial Differential Equations (Academic Press, Inc., New York, 1977).

VIII. ACKNOWLEDGMENTS